Glucosylceramide synthesis inhibition affects cell cycle progression, membrane trafficking, and stage differentiation in *Giardia lamblia*

Saša Štefanić,[1,*] Cornelia Spycher,[*] Laura Morf,[*] Gemma Fabriàs,[§] Josefina Casas,[§] Elisabeth Schraner,[†] Peter Wild,[†] Adrian B. Hehl,[2,*] and Sabrina Sonda[2,3,*]

Institute of Parasitology* and Institute of Veterinary Anatomy,[†] University of Zurich, Zurich, Switzerland; and Institut de Química Avançada de Catalunya,[§] Consejo Superior de Investigaciones Científicas (CSIC), Barcelona, Spain

Abstract Synthesis of glucosylceramide via glucosylceramide synthase (GCS) is a crucial event in higher eukaryotes, both for the production of complex glycosphingolipids and for regulating cellular levels of ceramide, a potent antiproliferative second messenger. In this study, we explored the dependence of the early branching eukaryote *Giardia lamblia* on GCS activity. Biochemical analyses revealed that the parasite has a GCS located in endoplasmic reticulum (ER) membranes that is active in proliferating and encysting trophozoites. Pharmacological inhibition of GCS induced aberrant cell division, characterized by arrest of cytokinesis, incomplete cleavage furrow formation, and consequent block of replication. Importantly, we showed that increased ceramide levels were responsible for the cytokinesis arrest. In addition, GCS inhibition resulted in prominent ultrastructural abnormalities, including accumulation of cytosolic vesicles, enlarged lysosomes, and clathrin disorganization. Moreover, anterograde trafficking of the encystations-specific protein CWP1 was severely compromised and resulted in inhibition of stage differentiation. Our results reveal novel aspects of lipid metabolism in *G. lamblia* and specifically highlight the vital role of GCS in regulating cell cycle progression, membrane trafficking events, and stage differentiation in this parasite. In addition, we identified ceramide as a potent bioactive molecule, underscoring the universal conservation of ceramide signaling in eukaryotes.—Štefanić, S., C. Spycher, L. Morf, G. Fabriàs, J. Casas, E. Schraner, P. Wild, A. B. Hehl, and S. Sonda. **Glucosylceramide synthesis inhibition affects cell cycle progression, membrane trafficking, and stage differentiation in *Giardia lamblia*. *J. Lipid Res.* 2010.** 51: **2527–2545.**

Supplementary key words ceramide • sphingolipid • cell division • vesicular trafficking

Sphingolipids are a highly complex class of lipids in terms of structural diversity, metabolism, and cellular functions. While initially seen as inert structural components of eukaryotic cell membranes, there is now substantial evidence that sphingolipids play an important role in signal transduction. (For a recent review on bioactive sphingolipids, see Ref. 1.)

Ceramide, a central molecule in the sphingolipid biosynthesis, plays a critical role as second messenger in cellular signaling that regulates antiproliferative processes, including apoptosis, cell differentiation, and cell cycle arrest in different cell types. Levels of ceramide, a highly bioactive molecule, must be tightly controlled by diverse, coordinated mechanisms, including ceramide degradation, phosphorylation, or sphingolipid metabolism. Glucosylceramide synthase (GCS), also defined as ceramide glucosyltransferase (CGT), metabolizes ceramide to glucosylceramide (GlcCer), a glycosylated form of ceramide that does not have antiproliferative activity. GCS plays a crucial role in cell survival after apoptotic stimuli,

This work was supported by grants from the Marie Heim-Vögtlin Foundation and the Fondation Pierre Mercier pour la Science, Switzerland (S. S); Swiss National Science Foundation Grant No. 112327 (A. B. H.); and fellowships (C.S.) from the Stiftung für Forschungsföderung of the University of Zurich, the Roche Research Foundation, and Novartis Stiftung für Medizin-Biologische Forschung. The Giardia lamblia microarrays (version 1) were kindly offered through the National Institute of Allergy and Infectious Diseases's Pathogen Functional Genomics Resource Center, managed and funded by the National Institutes of Health and operated by the J. Craig Venter Institute. The Functional Genomics Centre Zurich, Switzerland is a joint facility of the Eidgenössische Technische Hochschule Zürich and the University of Zurich.

Manuscript received 21 October 2009 and in revised form 23 March 2010.

Published, JLR Papers in Press, March 23, 2010
DOI 10.1194/jlr.M003392

Abbreviations: CTX, cholera toxin B subunit; CLH, clathrin; CWP, cyst wall protein; ER, endoplasmic reticulum; ESV, encystation-specific vesicle; GCS, glucosylceramide synthase; GlcCer, glucosylceramide; GlGCS, GlcCer synthase; PPMP, DL-threo-1-Phenyl-2-palmitoylamino-3-morpholino-1-propanol; PV, peripheral vesicle.

[1] Present address of S. Štefanić: Sandler Center for Basic Research in Parasitic Diseases, Mission Bay Campus, University of California, San Francisco, CA.

[2] To whom correspondence should be addressed.
e-mail: sabrina.sonda@usz.ch (S.S.);
adrian.hehl@access.uzh.ch (A.B.H.)

[3] Present address of S. Sonda: Pancreatitis Research Laboratory, Department of Visceral and Transplantation Surgery, University Hospital Zurich, Rämistrasse 100, DL36 8091 Zurich, Switzerland.

The online version of this article (available at http://www.jlr.org) contains supplementary data in the form of seven figures.

as demonstrated by the upregulation of GCS and GlcCer in some multidrug resistant tumor cells to counteract a chemotherapy-induced increase of ceramide (2, 3). Conversely, decreased GCS activity by RNA interference or by pharmacological inhibition of GCS activity with PPMP (DL-*threo*-1-Phenyl-2-palmitoylamino-3-morpholino-1-propanol) leads to ceramide buildup and cytotoxicity (4, 5). Thus, GCS is considered a pivotal regulator of bioactive ceramide levels.

Sphingolipid metabolism in pathogenic protozoa is the object of increasing interest as a source of promising chemotherapy targets. We recently showed that PPMP has a potent inhibitory effect on *Giardia lamblia* (6), a protozoan parasite that has undergone massive minimization during evolution (7) and that is a leading cause of intestinal infection worldwide (8). Both stages of the parasite's life cycle, namely, replicating trophozoites, which are responsible for pathogenesis, and environmentally resistant cysts, which are responsible for disease transmission, were affected by PPMP at concentrations that are not toxic for mammalian cells. The observed sensitivity to PPMP suggested that an active GCS may exist in the parasite; in addition, a GCS homolog, GL50803_11642, is annotated in the *G. lamblia* Genome Database (http://giardiadb.org), and its transcription has been reported to be regulated during the parasite's life cycle (9). Moreover, the predicted ORF GL50803_7598 contains a domain typical of the glycolipid transfer protein (GLTP) superfamily. While the precise cellular function of GLTP remains undefined, a proposed correlation between the presence of GLTP and GCS activity (10) further supports the presence of active GCS in the parasite.

However, the synthesis of sphingolipids and of GlcCer in particular has not been demonstrated in the parasite so far. Lipid neosynthesis is limited in *G. lamblia*, and the parasite is thought to rely on lipids taken up from the environment, namely, the host intestinal content. Indeed, in vitro analyses showed negligible incorporation of lipid precursors, such as acetate and glycerol (11), while robust incorporation of exogenous radiolabeled fatty acids (12–14), phospholipids (14), ceramide, and gangliosides (15, 16) could be demonstrated. In addition, uptake of fluorescent sphingolipid analogs, including ceramide and sphingomyelin, has been reported (12, 14, 15). Importantly, acyl chain desaturation (17), deacylation/reacylation, and head group exchange (18) have been shown to occur in *G. lamblia*, indicating that the parasite can remodel the incorporated exogenous lipids to fulfill its own needs.

In this study, we used a biochemical approach to address whether the synthesis of GlcCer occurs in *G. lamblia* and whether it can be inhibited by PPMP. In addition, we investigated the molecular mechanism of PPMP-mediated effects in more detail and identified ceramide as a key modulator of cellular processes in this parasite.

MATERIALS AND METHODS

Biochemical reagents

Unless otherwise stated, all chemicals were purchased from Sigma and cell culture reagents from Gibco-BRL. Inhibitor stock solutions were prepared at the following concentrations: 10 mM DL-*threo*-1-Phenyl-2-palmitoylamino-3-morpholino-1-propanol (PPMP), 14 mM fumonisin B1 (FB1), 5 mM myriocin (Myr), 250 mM L-cycloserine (L-cyc), 22.5 mM N-butyldeoxynojirimycin (NB-DNJ), 3 mM tunicamycin (TM), 16.6 mM nocodazole, and 20 mg/ml puromycin. Inhibitors were freshly diluted to the concentrations required for the individual experiment.

Parasite cell culture

Trophozoites of the *Giardia lamblia* strain WBC6 (ATCC catalog number 50803) were grown axenically as described (6). Harvested parasites were counted using the improved Neubauer chamber. New subcultures were obtained by inoculating 5×10^4 trophozoites from confluent cultures into new 11 ml culture tubes.

Two-step encystation was induced as described previously (19, 20) by cultivating the cells for ~44 h in medium without bile (pre-encysting medium) and subsequently in medium with higher pH and porcine bile (encysting medium).

Drug treatment of trophozoites was performed on freshly inoculated subcultures. Parasites were allowed to adhere for 8 h and then incubated for additional 16 h with the inhibitors at the concentrations indicated in the figure legend of the individual experiments. Drug treatment of encysting cells was performed in two steps: 7 h drug incubation in pre-encysting medium and additional 16 h incubation in encysting medium. For replication and doublet formation assay, cells were harvested and counted as described above.

For reversibility assay, freshly inoculated subcultures were incubated with the inhibitor for 16 h as described above, harvested, and washed to remove the drug. Collected parasites were then counted and reinoculated in absence of inhibitor for an additional 4 days, followed by counting.

Expression vector construction and transfection

All constructs of giardial glucosylceramide synthase (GCS) (GL50803_11642) were based on the expression cassette C1-CWP for inducible expression under the control of the CWP1 promoter (19). For N-terminal tagging with the hemagglutinin (HA) epitope, full length GCS (aa 2–537) and variant without putative signal peptide (aa 23–537) coding regions were amplified by PCR and cloned in a vector containing the HA epitope tag upstream of the *NsiI* restriction site. For C-terminal tagging, the HA epitope tag was encoded on the antisense primer and the product cloned into an identical vector variant devoid of N-terminal HA-tag. Because the giardial GCS coding sequence contains an *NsiI* restriction site, a complementary *SbfI* restriction site was encoded on sense primers and used for ligation into the vectors.

Stable chromosomal integration of the described constructs was performed using the pPacV-Integ expression vector (21) using *XbaI* and *PacI* restriction sites. Oligonucleotides (5′-3′ orientation) used in this study were: GCS(2-537)-*SbfI*-s AGATCTCCTGCAGGACGGGTTGACTCTCTCCTTAGTG; GCS(23-537)-*SbfI*-s AGATCTCCTGCAGGCTGTCAACCGCATAAGTG; GCS-*PacI*-as CGTTAATT AATCAGTCGAGGGATTTTTTATTGGCCTG;GCS-HA-*PacI*-asCGTTAATTAATCACGCGT AGTCTGGGACATCGTATGGGTAGTCGAGGGATTTTTTATTGGCCTG.

Plasmid vector DNA was linearized using *SwaI* restriction enzyme and 15 μg of digested plasmid DNA was electroporated (350V, 960μF, 800Ω) into trophozoites. Linearized plasmid targets the *G. lamblia* triose phosphate isomerase locus (GL50803_93938), and integration occurs by homologous recombination under selective pressure with the antibiotic puromycin (22).

Gene expression analysis

RNA was isolated from trophozoites or parasites allowed to encyst for 7 h using an RNAeasy kit (Qiagen, Stanford, CA) following

the "Animal Cells Spin" protocol. Residual genomic DNA was removed with DNase 1 digestion according to the manufacturer's protocol. The integrity of the RNA was analyzed in a Bioanalyser (Agilent Technologies Inc., Palo Alto, CA) with "Eukaryote Total RNA Nano Series II" settings.

For dual channel microarray analysis, extracted total RNA was processed using the "Amino Allyl MessageAmp™ II a RNA Amplification Kit"(Ambion, Austin, TX) and labeled with N-hydroxysuccinimidyl ester-derivatized reactive dyes Cy™3 or Cy™5, according to the manufacturer's protocol. After purification, 2 μg each of Cy3 or Cy5 labeled aRNA were denatured, added to SlideHyb™ Buffer I (Ambion), and hybridized to *G. lamblia* microarrays version 1 (TIGR) in a Tecan HybStation at the Functional Genomics Centre, Zurich, Switzerland. The arrays are epoxy surface coated glass slides with ss-oligo (70 mers) containing 19,230 elements and covering the whole *G. lamblia* WBC6 strain genome.

Before hybridization, slides were hydrated and blocked with 150 μl Tris-HCl-ethanolamine (0.1 M Tris, 50 mM ethanolamine, pH 9.0), for 30 min at 50°C. After washing, samples were injected and hybridized for 16 h at 42°C. Slides were scanned in an Agilent Scanner G2565AA, using laser lines 543 nm and 633 nm for excitation of Cy3 and Cy5, respectively. Spatial scanning resolution was 10 μm, single pass. The scanner output files were quantified using the Genespotter Software (MicroDiscovery GmbH, Berlin, Germany) with default settings and 2.5 μm radius. The median spot intensities were evaluated with the Web application MAGMA (23) and normalized using the print-tip-wise loess correction of the *limma* package (24). Potential gene-specific dye-effects were estimated from self-self hybridizations. Differential expression of genes during encystation is reported as encystation-induced fold-change, as well as the *P* value for differential expression as estimated by the empirical Bayes model implemented in *limma*. Experiments were performed in biological triplicate.

For semiquantitative real-time PCR, first strand cDNA synthesis was performed using ~350 ng RNA and Omniscript reverse transcriptase (Qiagen), according to manufacturer's protocol. Amplification was performed in an iCycler iQ (Biorad, Hercules, CA) using 2 μl of 1:1000 diluted cDNA. To monitor possible contamination with residual genomic DNA, PCR amplification was performed on the extracted RNA and water. Primer pairs (5′-3′ orientation) used for amplification of actin (ACT), cyst wall protein 1 (CWP1), and GCS were ACT-s, ACATATGAGCTGCCAGATGG; ACT-as,TCGGGGAGGCCT GCAAAC; CWP1s,-GGCGATATTCCCGAGTGCATGTG; CWP1as,GTGAGGCAGTACTCTA GT; GCS-s, GCAGACCAAGCCTAGCATC; and GCS-as, CCTTTACCACAGGCACTTTG. All reactions were run in triplicate. To assess the efficiency of the amplification reactions, standard curves for every primer pair and cDNA were generated from 6-fold serial dilutions in duplicate, using the iQ5 software. Expression levels of the genes were given as values in arbitrary units relative to the amount of the constitutively expressed housekeeping gene actin.

Lipid analysis

For analysis of lipid synthesis in *G. lamblia* in presence of inhibitors, isolated parasites were pretreated with the selected compounds for 30 min at 37°C followed by labeling with 4 μCi/ml [^{3}H]palmitic acid or [^{3}H]serine for 3 h at 37°C in supplemented PBS (PBS containing 50 mM glucose, 9 mM L-cysteine, 1.7 mM ascorbic acid, pH 7.1) in presence of the compounds. Labeling with 20 μCi/ml [^{3}H]glucose was performed in supplemented PBS without glucose addition. After extensive washing with PBS and 0.05% fat-free BSA in PBS, lipids were extracted according to (25). Extracted lipids were saponified by mild alkaline hydrolysis when required. Lipid aliquots were separated by high-performance, thin-layer chromatography (HPTLC) on Silica Gel 60 plates. Solvent systems used were the following: A, first dimension, chloroform:methanol:25% ammonium hydroxide:water (65:35:4:4); second dimension, chloroform:aceton:methanol:acetic acid:water (50:20:10:10:5); B, chloroform:methanol:25% ammonium hydroxide (65:25:4.5); C, chloroform:methanol:acetic acid:water (84:4.5:5:0.5) D, benzene:2-propanol:water (100:10:0.25). Radiolabeled bands were visualized using a tritium-sensitive screen (Perkin-Elmer, Boston, MA) in a Personal Molecular PhosphoImager FX (Biorad), identified according to comigrating standards (Avanti Polar Lipids, Alabaster, AL) visualized by iodine vapors and quantified using ImageQuant software (Amersham, Otelfingen, Switzerland).

For ceramide glycanase digestion, samples were dissolved in 50 mM sodium acetate buffer pH 5.0 containing 0.1% (w/v) sodium cholate. Ceramide glycanase (Calbiochem) was added at 3.1 U/ml, and digestion was performed at 37°C for 24 h. Lipids were extracted and analyzed by TLC.

For radioactivity incorporation analysis, parasites were labeled with radioactive precursors as described. Cell aliquots were solubilized with 0.1N NaOH or processed for lipid extraction; whole cell- or lipid-associated radioactivity was measured by liquid scintillation and normalized by protein content.

Liquid chromatography-mass spectrometry (LC-MS) was carried out using lipids from *G. lamblia* trophozoites, with or without PPMP treatment, and 24 h encysted cells containing an average of 33% cysts, as described (26). Briefly, cells were harvested, washed in PBS, and transferred to glass vials. Sphingolipid extracts, fortified with internal standards (N-dodecanoylsphingosine, N-dodecanoylglucosylsphingosine, and N-dodecanoylsphingosylphosphorylcholine, 0.5 nmol each), were prepared as described (27) and analyzed. The liquid chromatography-mass spectrometer consisted of a Waters Aquity UPLC system connected to a Waters LCT Premier orthogonal accelerated time of flight mass spectrometer (Waters, Millford, MA), operated in positive electrospray ionization mode. Full scan spectra from 50 to 1500 Da were acquired, and individual spectra were summed to produce data points each 0.2 s. Mass accuracy and reproducibility were maintained by using an independent reference spray by the LockSpray interference. The analytical column was a 100 mm × 2.1 mm i.d., 1.7 μm C8 Acquity UPLC BEH (Waters). The two mobile phases were A: methanol:water:formic acid (74:25:1); B: methanol:formic acid (99:1), both also contained 5 mM ammonium formate. A linear gradient was programmed as follows: 0.0 min: 80% B; 3 min: 90% B; 6 min: 90% B; 15 min: 99% B; 18 min: 99% B; 20 min: 80% B. The flow rate was 0.3 $mlmin^{-1}$. The column was held at 30°C. Quantification was carried out using the extracted ion chromatogram of each compound, using 50 mDa windows. The linear dynamic range was determined by injecting standard mixtures. Positive identification of compounds was based on the accurate mass measurement with an error <5 ppm and its LC retention time, compared with that of a standard (±2%).

Fluorescence microscopy analysis

Lysotracker Blue-White (Molecular Probes) staining of live trophozoites was performed at 100 nM in supplemented PBS at 37°C for 1 h. Cells were then resuspended in PBS and directly imaged.

For surface labeling, parasites were incubated with 6 μg/ml fluorescein-conjugated cholera toxin B subunit (Molecular Probes) in supplemented PBS for 60 min at 4°C and analyzed after fixation in 3% formaldehyde solution in PBS for 45 min on glass slides.

For membrane endocytosis, parasite were incubated with cholera toxin for 30 min at 4°C, washed in PBS, incubated at 37°C for the time indicated in the figure legends, and imaged after fixation. Endocytosis was quantified by counting the percentage of cells stained in the endocytosis signature area at the center of the ventral disk.

For immunolabeling, cells were harvested as described above, washed twice in ice-cold PBS, and fixed as before on glass slides. Fixed cells were permeabilized with 0.2% Triton X-100 in PBS for 20 min, blocked, and incubated with primary antibodies for 1 h. The primary antibodies used in this study were anti-clathrin heavy chain (CLH) mouse antiserum (28), 1:2000 dilution; anti-protein disulfide isomerase 2 (PDI2) mouse antiserum, 1:1000 dilution; Cy3-conjugated anti-cyst wall protein 1 (CWP1) mouse monoclonal antibody (Waterborne, New Orleans, LA), 1:60 dilution; and Alexa488-conjugated anti-HA mouse monoclonal antibody (Roche Diagnostics GmbH, Manheim, Germany) 1:30 dilution. Fluorophore-conjugated secondary antibodies were purchased from Invitrogen (Basel, Switzerland) and used at 1:200 dilution. Microscopy analyses were performed on a Leica DM IRBE fluorescence microscope or on a Leica SP2 AOBS confocal laser-scanning microscope (Leica Microsystems, Wetzlar, Germany), using the appropriate settings. Image stacks of optical sections were further processed using the Huygens deconvolution software package version 2.7 (Scientific Volume Imaging, Hilversum, The Netherlands). Three-dimensional reconstruction and surface rendering was done with the Imaris software suite (Bitplane, Zurich, Switzerland) using the surpass functions.

Electron microscopy analysis

Parasite were treated with PPMP or solvent for 16 h and collected as described. The cells were resuspended in 2.5% glutaraldehyde in 0.1M Na/K-phosphate, pH 7.4, and centrifuged at 3500 *g* for 20 min. After washing, pellets were postfixed with 1% osmium tetroxide in 0.1M Na/K-phosphate for 1 h, dehydrated in a graded ethanol series, transferred to acetone for embedding in epon, and polymerized at 60°C for 2.5 days. Ultrathin sections were stained with uranyl acetate and lead citrate and examined at an acceleration voltage of 100 kV in a Philips CM 12 transmission electron microscope (Eindhoven, The Netherlands) equipped with a low-scan CCD camera (Gatan, Pleasanton, CA).

Determination of protein concentration

Protein content was determined using the Bio-Rad Protein Assay according to the instructions provided by the manufacturer. Bovine serum albumin was used for the standard curve.

RESULTS

PPMP inhibits glucosylceramide synthesis and increases ceramide levels in *G. lamblia*

In mammalian cells, PPMP blocks the synthesis of GlcCer by occupying the catalytic site of GCS, the enzyme that transfers one glucose molecule to ceramide. PPMP treatment results in decreased cellular levels of GlcCer and accumulation of the ceramide precursor (29). To determine whether *G. lamblia* is capable of GlcCer synthesis and whether PPMP inhibits GlcCer formation in the parasite, we metabolically labeled *G. lamblia* trophozoites and analyzed the extracted lipids by two-dimensional thin-layer chromatography (2D TLC). Labeling with the [^{3}H]palmitic acid precursor showed that 10 μM PPMP, a concentration we previously showed to inhibit *G. lamblia* replication (6), strongly altered the lipid profile by either decreasing (**Fig. 1A**, spots A, B) or increasing (spots C, D) the abundance of labeled lipids or inducing the appearance of labeled species not visible in the untreated sample (spot E). Saponification of extracted lipids by mild alkaline hydrolysis to remove glycerol-based lipids revealed

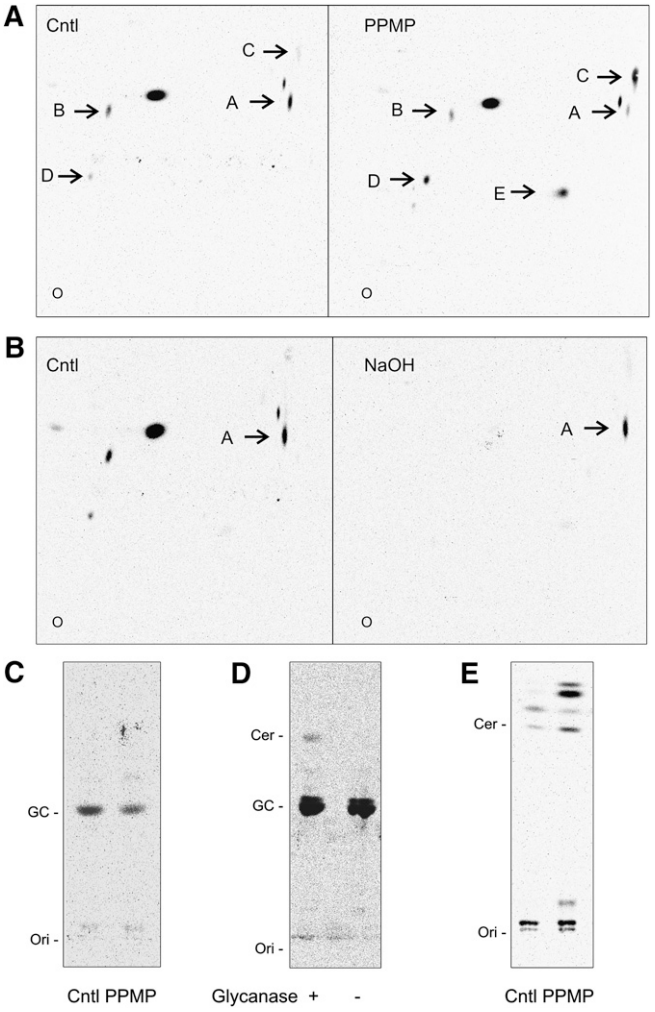

Fig. 1. PPMP inhibits GlcCer synthesis in *G. lamblia*. Isolated parasites were labeled with [^{3}H]palmitic acid for 3 h in presence of 10 μM PPMP or solvent (cntl). A: Lipid aliquots corresponding to equal protein amount were separated by 2D-HPTLC using the solvent system A. Note the decreased (spots A, B) or increased (spots C, D, E) abundance of labeled lipids in presence of the inhibitor. B: Saponification of extracted lipids by mild alkaline hydrolysis (NaOH) and separation as described before revealed that lipid "A" belongs to the sphingolipids class. C: Saponified lipid aliquots corresponding to equal protein amount were separated by 1D-HPTLC using the solvent system B. Note the decreased amount of the band comigrating with a GlcCer standard (GC) upon 10 μM PPMP treatment. D: Spot A was cut from the TLC and hydrolyzed with ceramide glycanase, as described in "Materials and Methods." Samples were then separated by 1D-HPTLC using the solvent system B. E: 1D-HPTLC of lipids corresponding to equal protein amount using the solvent system C for ceramide (Cer) separation. Note the ceramide increase upon 10 μM PPMP treatment. O, Ori, origin.

that lipid "A" was resistant to the treatment, thus supporting that it belongs to the sphingolipid class (Fig. 1B). In addition, 1D TLC of saponified samples showed that the predominant band comigrated with a GlcCer standard and its amount decreased upon PPMP treatment (Fig. 1C), supporting the notion that lipid "A" is GlcCer. To further confirm that lipid "A" is indeed GlcCer, the spot was cut from the TLC and tested for sensitivity to ceramide glycanase, which hydrolyzes the glucose moiety from glycosphingolipids. While the hy-

drolysis was not complete, TLC separation revealed a band comigrating with ceramide in the glycanase-treated sample (Fig. 1D), indicating that the lipid in spot "A" is a substrate for the enzyme.

Having confirmed that PPMP treatment decreased the synthesis of GlcCer in *G. lamblia*, we next monitored whether GlcCer synthesis inhibition resulted in increased cellular levels of the precursor ceramide. TLC separation showed that a band comigrating with ceramide standard is indeed more abundant in the PPMP-treated sample (Fig. 1E). Similar to the PPMP-mediated inhibition of *G. lamblia* replication (6), PPMP inhibition of GlcCer synthesis was dose-dependent (**Fig. 2A**). Importantly, GlcCer synthesis was reduced even in cells only pretreated with 10 μM PPMP for 30 min before drug removal and metabolic labeling (Fig. 2A, Pre), suggesting that the inhibitory effect is not reversible.

Finally, we quantified the reduction of the total GlcCer cellular pool following PPMP treatment. Mass spectrometry analysis readily identified the presence of GlcCer in the parasite (supplementary Fig. I). PPMP treatment for 4 h significantly reduced the amount of less abundant GlcCer species (18:0 and 20:0). Of note, the abundance of GlcCer species containing long fatty acid residues (22:0 and 24:0) did not vary in PPMP-treated cells, suggesting a different rate of lipid turnover for different GlcCer pools (Fig. 2B). Overall, our data show that, similar to mammalian cells, PPMP inhibited GlcCer synthesis, resulting in increased cellular levels of ceramide in *G. lamblia*.

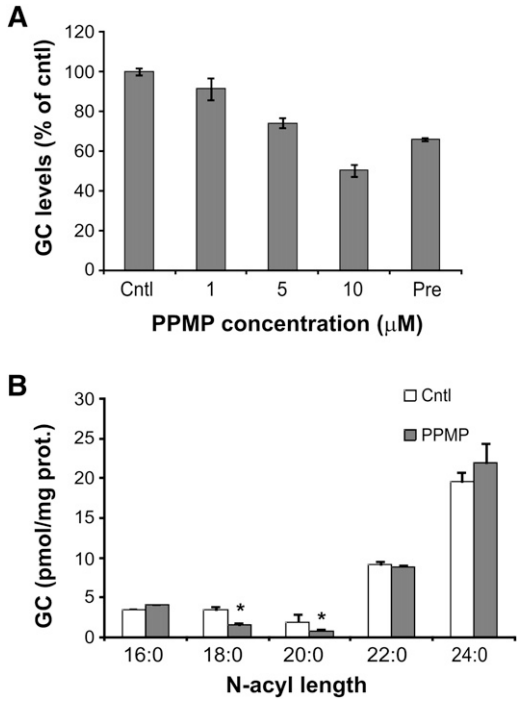

Fig. 2. Dose-response inhibition of GlcCer synthesis following PPMP treatment. A: Isolated parasites were labeled with [^{3}H]palmitic acid for 3 h in presence of solvent (cntl) or PPMP at the indicated concentrations. Alternatively, parasites were pretreated with 10 μM PPMP for 30 min, washed, and labeled with [^{3}H]palmitic acid as described before (Pre). Lipid aliquots corresponding to equal protein amount were separated by 1D-HPTLC using the solvent system B. GlcCer (GC) levels are expressed as percentage of untreated samples (cntl); data are average ± SE (n = 3) of a representative from two experiments done in triplicate. B: Liquid chromatography-mass spectrometry analysis of glucosylceramides extracted from trophozoites treated for 4 h with of 10 μM PPMP or solvent (cntl). Data are average ± SE (n = 3). *A significant difference ($P < 0.05$) compared with the percentage of control treated parasites, two-tailed Student's *t*-test.

Metabolic labeling of *G. lamblia* sphingolipids

G. lamblia is considered to have a limited capability for de novo lipid synthesis (30), and only a few candidate enzymes of the sphingolipid synthetic pathway are annotated in the parasite genome (9). Thus, it is not known whether the parasite is able to carry out a complete de novo synthesis of sphingolipids or if it relies solely on host-derived lipid precursors and/or preformed complex lipids. To determine whether GlcCer in cultured *Giardia* trophozoites derives from de novo synthesized ceramide or from remodeling of ceramide taken up from the medium, we metabolically labeled the cells with [^{3}H]serine, a substrate for serine palmitoyl transferase (SPT), the first committing enzyme of sphingolipid synthesis, which is also annotated in the giardial genome (supplementary Fig. II). Serine was incorporated in the parasite three times less efficiently than palmitic acid (supplementary Fig. III) and labeled one major and few minor lipid species, which comigrated neither with ceramide (**Fig. 3A**) nor with GlcCer (Fig. 3B). In contrast with [^{3}H]palmitic acid labeling, all serine-labeled species were alkali-sensitive and, thus, glycerol-based lipids (Fig. 3B). Therefore, under these experimental conditions, serine did not label *G. lamblia* sphingolipids, suggesting that the observed ceramide labeling with [^{3}H]palmitic acid is likely to derive from deacylation/reacylation reactions on a preexisting ceramide pool.

To further elucidate the modality of sphingolipid synthesis, we performed cell labeling with [^{3}H]glucose. This labeled molecule was only weakly incorporated into the lipid fraction of *G. lamblia*, accounting for 6% of the whole cell-associated radioactivity (**Fig. 4B**). However, a band comigrating with parasite GlcCer was clearly visible after prolonged TLC exposure (Fig. 3C). Similar to the observations during [^{3}H]palmitic acid labeling, PPMP treatment diminished the labeling of GlcCer and increased the intensity of other labeled species.

G. lamblia GlcCer synthesis is not modulated by other sphingolipid inhibitors but by tunicamycin

While SPT, a homolog of the first committing enzyme of sphingolipid synthesis, is found in *G. lamblia*, the other enzymes in the ceramide biosynthesis pathway have not been annotated in the parasite's genome, suggesting that giardial sphingolipid synthesis is incomplete. We then tested whether known inhibitors of these early steps of sphingolipid synthesis (31) (supplementary Fig. II) may inhibit GlcCer formation in the parasite. We performed lipid metabolic analyses in the presence of compounds interfering with *i*) the first committed step of sphingolipid synthesis (20 μM myriocin and 500 μM L-cycloserine), *ii*) the synthesis of ceramide (50 μM fumonisin B1), and *iii*) an additional inhibitor of GCS, structurally unrelated to PPMP

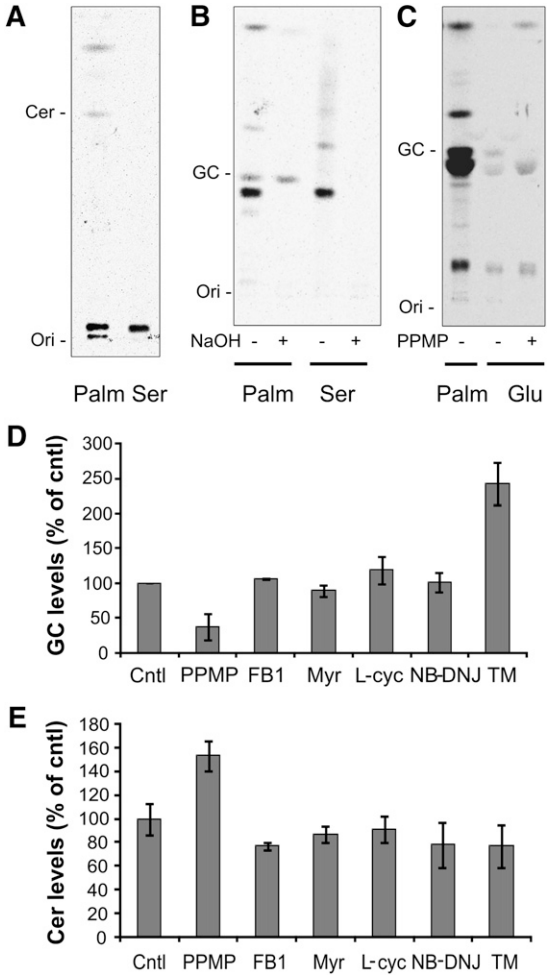

Fig. 3. *G. lamblia* incorporates [^{3}H]glucose but not [^{3}H]serine in GlcCer. A: Isolated parasites were labeled with [^{3}H]palmitic acid (Palm) or [^{3}H]serine (Ser) for 3 h and the extracted lipids separated by 1D-HPTLC using the solvent system C. For serine-labeled samples, lipid aliquots corresponding to three times the protein amount of palmitic acid-labeled samples were used to compensate for the reduced incorporation efficiency. Note the absence of ceramide labeling with serine. B: Extracted lipids were saponified by mild alkaline hydrolysis (NaOH) and separated using the solvent system B. Note the complete hydrolysis of the serine-labeled lipids. C: Parasites were labeled with [^{3}H]glucose in presence of 10 μM PPMP or solvent alone. Extracted lipids were separated using the solvent system B. Note the decreased amount of the band comigrating with GlcCer upon PPMP treatment. Ori, origin. D: Isolated parasites were labeled with [^{3}H]palmitic acid for 3 h in presence of solvent (cntl), 10 μM PPMP, 50 μM fumonisin B1 (FB1), 20 μM myriocin (Myr), 500 μM L-cycloserine (L-cyc), 400 μM NB-DNJ, and 60 μM tunicamycin (TM). Lipid aliquots corresponding to equal protein amount were separated by 1D-HPTLC using the solvent system B or C (panel E). GlcCer (GC) and ceramide (Cer) levels are expressed as percentage of untreated samples (cntl); data are average ± SE (n = 3) of a representative from three experiments done in triplicate. Note the opposite effect of PPMP and TM treatment on GlcCer levels.

(400 μM NB-DNJ). In addition, we tested 60 μM tunicamycin, an amphipatic analog of UDP-GlcNAc, which was shown to inhibit the synthesis of complex glycosphingolipids in mammalian cells by blocking sugar import into the Golgi apparatus (32–34). All inhibitors were used at the highest concentration of the range used to affect mammalian sphingolipid synthesis.

Interestingly, of all the sphingolipid inhibitors tested, only PPMP was found to decrease GlcCer (Fig. 3D) and to increase ceramide levels (Fig. 3E), while the other compounds did not alter the synthetic capability of the parasite. On the other hand, tunicamycin treatment was found to increase the GlcCer content without affecting ceramide levels (Fig. 3D, E; supplementary Fig. IV), suggesting that sphingolipid synthesis in the parasite is sensitive to compounds interfering with cellular sugar transport.

Inhibition of GlcCer synthesis promotes lipid turnover

Our previous experiments using tritiated palmitic acid and glucose showed that PPMP increased the labeling of several lipid species different from GlcCer. Such an increase was further quantified by liquid scintillation analysis of the incorporated radioactivity. [^{3}H]palmitic acid incorporation increased both in whole cells and in the lipid fraction of PPMP-treated parasites compared with control cells (Fig. 4A), suggesting that the increased lipid incorporation is accompanied by an increased precursor uptake. Interestingly, [^{3}H]glucose incorporation increased in the lipid fraction but not in whole cell extracts (Fig. 4A). To test whether palmitic acid and glucose were differently metabolized into lipids, we quantified the percentage of whole cell-associated precursors found in the lipid fraction. The majority (80%–90%) of the cell-associated [^{3}H]palmitic acid was identified in the lipid fraction also after PPMP treatment. Conversely, only 6% of the cell-associated [^{3}H]glucose was found in the lipid fraction, confirming the limited glucose incorporation reported by Jarroll et al (11). However, the amount of lipid-associated glucose increased by 70% in presence of PPMP, suggesting that the intracellular glucose pool is relocated toward a lipid synthetic use (Fig. 4B).

The previously described inhibitors (Fig. 3D, E) were similarly tested in their capability to modulate [^{3}H] palmitic acid incorporation in *G. lamblia* extracts. Consistent with the demonstrated absence of sphingolipid synthesis inhibition, none of the sphingolipid inhibitors altered the incorporation of the labeled precursor into either whole cells or lipids (Fig. 4C).

To identify other lipid classes whose synthesis may be modulated upon PPMP inhibition of GlcCer synthesis, we analyzed the pattern of neutral lipids labeled with [^{3}H]palmitic acid. While 1,2 and 1,3 diacylglycerols (DAG) were the main species present in untreated cells, PPMP treatment dramatically changed the proportion of these lipids, increasing 1,2 DAG levels and reducing 1,3 DAG (Fig. 4D, parts a, b). The observed alteration of neutral lipid synthesis may have been triggered by reduced GlcCer synthesis or increased ceramide levels in PPMP-treated cells. To discriminate between these possibilities, we increased ceramide levels using cell-permeable C6 ceramide. In these experimental conditions we observed an increase in both 1,2 DAG content (Fig. 4D, parts a, b) and 1,2 and 1,3 DAG ratio (Fig. 4D, part c), indicating that increased ceramide levels contribute to the observed modulation of neutral lipids.

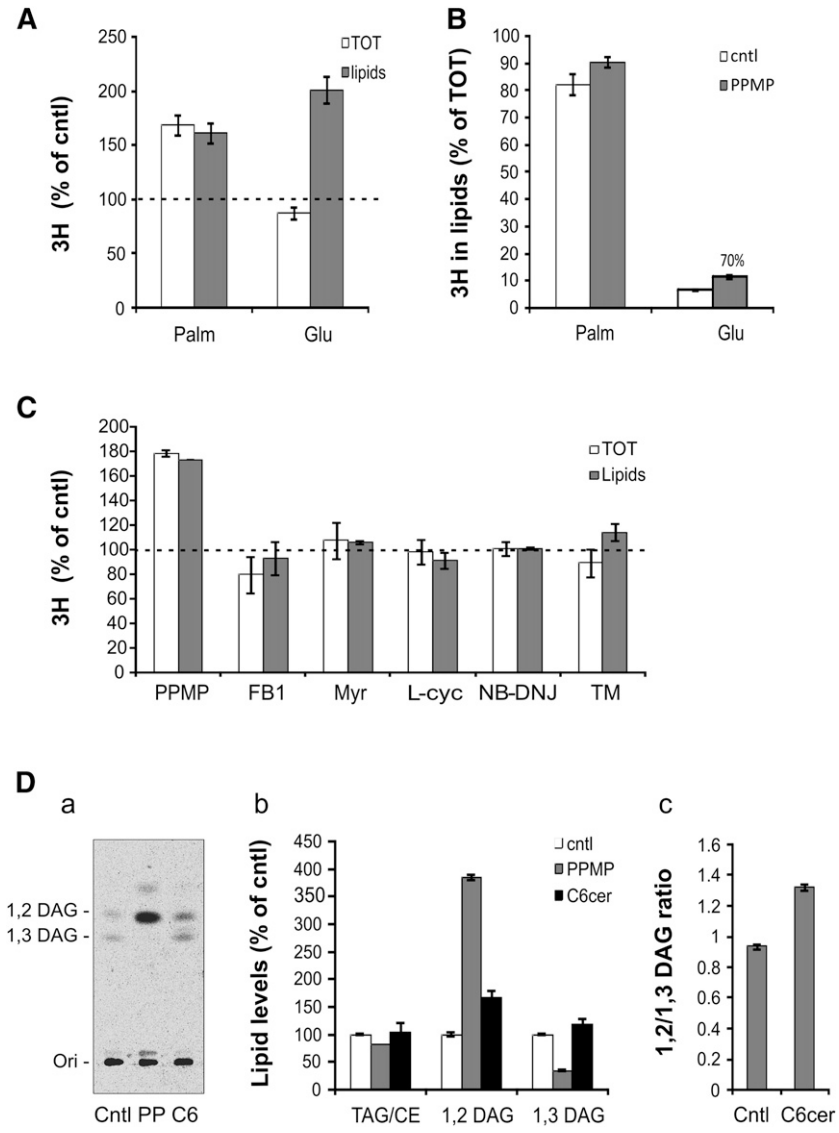

Fig. 4. Inhibition of GlcCer synthesis promotes *G. lamblia* lipid turnover. Isolated parasites were labeled with [^{3}H]palmitic acid or [^{3}H]glucose for 3 h in presence of solvent (cntl) or 10 μM PPMP. [^{3}H] incorporation was measured in both whole cell (TOT) and lipid extracts by liquid scintillation and normalized by protein content. A: Incorporation is expressed as percentage of untreated samples (cntl, dashed line); data are average ± SE (n = 9) of three experiments done in triplicate. Note that PPMP treatment increased [^{3}H] palmitic acid incorporation both in whole cells and in the lipid fraction, while only in the lipid fraction in the case of [^{3}H]glucose. B: [^{3}H] incorporation in the lipid fraction is expressed as percentage of whole cell-associated precursors. Note the readily incorporation into lipids of [^{3}H]palmitic acid, compared with [^{3}H] glucose and the increased [^{3}H]glucose incorporation upon PPMP treatment. C: Comparison of [^{3}H]palmitic acid incorporation in *G. lamblia* extracts as described in panel A upon treatment with solvent (cntl), 10 μM PPMP, 50 μM fumonisin B1 (FB1), 20 μM myriocin (Myr), 500 μM L-cycloserine (L-cyc), 400 μM NB-DNJ, and 60 μM tunicamycin (TM). Incorporation is expressed as percentage of untreated samples (cntl, dashed line); data are average ± SE (n = 9) of three experiments done in triplicate. D: Isolated parasites were labeled with 4 μCi/ml of [^{3}H]palmitic acid for 3 h in presence of solvent (cntl), 10 μM PPMP (PP) or 500 μM C6 ceramide (C6). Lipid aliquots corresponding to equal protein amount were separated using the solvent system D. (a) Representative 1D-HPTLC. DAG, diacylglycerols, Ori, origin. (b) Quantification of lipid levels expressed as percentage of untreated samples (cntl); data are average ± SE (n = 6) of two experiments done in triplicate. (c) Ratio of 1,2 and 1,3 DAG upon C6 ceramide treatment. Data are average ± SE (n = 6) of two experiments done in triplicate. Note the increase in 1,2 DAG level in PPMP and C6 ceramide treated samples.

Increased ceramide levels inhibit *G. lamblia* cell division

In our previous work, we showed that micromolar concentrations of PPMP arrested parasite cytokinesis and induced the accumulation of partially divided cells in the culture (6). To directly correlate the replication inhibition with the alteration of sphingolipid synthesis induced by PPMP, we raised the ceramide levels in *G. lamblia* using cell-permeable C6 ceramide, thus mimicking PPMP-induced

ceramide increase. Incubation with micromolar concentrations of exogenous C6 ceramide severely inhibited *G. lamblia* replication in a dose-dependent manner, with 30 μM completely arresting parasite division (**Fig. 5A**, white bars). Importantly, the concomitant presence of PPMP further inhibited parasite replication, indicating that ceramide and PPMP act as agonists on a cellular process that is involved in parasite replication (Fig. 5A, gray and black bars). Furthermore, quantitative analysis of C6 ceramide-treated parasites revealed that exogenous ceramide induced a cytokinesis arrest and accumulation of partially divided cells comparable to the one observed during PPMP treatment (Fig. 5B), indicating that increased ceramide levels are sufficient to inhibit *G. lamblia* cell division.

Similar to the observations described in the lipid analyses above, PPMP was unique among the sphingolipid inhibitors tested in both blocking parasite replication (Fig. 5C) and increasing the amount of partially divided cells (Fig. 5D), while the other inhibitors affected neither sphingolipid synthesis (Fig. 3D, E) nor parasite cell division (Fig. 5C, D). Furthermore, tunicamycin treatment, which increased cellular GlcCer levels, did not alter parasite replication and doublet formation, suggesting that increased GlcCer levels alone are not sufficient to promote cell division.

We investigated the effect of PPMP on cell division in more detail and found that the inhibitor exerted a long-term block of *G. lamblia* replication after its removal from the culture medium. Parasites treated with the inhibitor for 16 h could not resume cell division even 4 days after PPMP removal, whereas control cells reached the density plateau at day 3 (Fig. 5E). The plasma membrane of treated parasites was visualized with fluorescein isothiocyanate-conjugated cholera toxin (CTX), which binds to the raft-associated sphingolipid GM1 (35). CTX staining revealed that cytokinesis-arrested parasites had properly formed ventral disks (Fig. 5F, arrowheads), but the cleavage furrow was mainly absent or, in a minority of cases, incomplete (Fig. 5F, arrows).

Ultrastructural abnormalities following inhibition of GlcCer synthesis

To examine the ultrastructure of *G. lamblia* upon inhibition of GlcCer synthesis, we compared control cells with PPMP-treated parasites by thin-section transmission electron microscopy. Consistent with our previous light microscopy observations, we observed an accumulation of partially divided cells in the PPMP-treated samples. In addition, in comparison with untreated cells (**Fig. 6E**), vesicles bounded by single lipid bilayer membranes accumulated within the cytosol of PPMP-treated parasites (Fig. 6A, arrows and magnified images). Such vesicles had a size of 60–100 nm and a non-homogeneous electron-density different from the one observed in peripheral vesicles (PV). The vesicles were present as clusters beneath the plasma membrane in close proximity with the PVs, juxtaposed to the nuclear envelope, or in the cell interior. PPMP-treated parasites also contained conspicuous electron-lucent vacuoles of various diameters (Fig. 6A–C, arrowheads), often located at the posterior end of the parasites. In addition, several vacuoles containing parasite flagella were observed (Fig. 6C, asterisks), which have been reported to occur in *G. lamblia* (36) and other anaerobic protists (37) under stress conditions.

Finally, PVs looked generally more distended in PPMP-treated cells (Fig. 6D), and coiled multilamellar structures were also observed, although infrequently (supplementary Fig. V). No gross alterations of parasite morphology, such as membrane blebbing, ventral disk fragmentation, or electron dense deposits were observed following PPMP treatment.

Inhibition of GlcCer synthesis perturbs clathrin localization and endolysosomal compartments, but does not inhibit membrane endocytosis

We hypothesize that vesicle accumulation detected in *G. lamblia* by electron microscopy may result from altered vesicular trafficking as a consequence of exposure to the drug. This hypothesis prompted us to investigate whether PPMP treatment affected the morphology of organelles involved in intracellular trafficking processes. First, we visualized the parasite clathrin (CLH), which is found closely associated with PVs (28), the endolysosome system of the parasite (28, 38). In control cells, the anti-CLH antibody stained punctate structures, which were uniformly distributed on the dorsal side of the parasite and clustered in selected areas on the ventral side, including the area at the center of the ventral disk (arrow), a signature site for endocytosis (39) (**Fig. 7A**). PPMP treatment significantly altered the staining pattern and induced aggregation of the punctate structures in the form of elongated or circular clusters.

Next, we monitored the cellular distribution of acidic compartments, including PVs, in living cells after incubation with lysotracker™ (Fig. 7B). While lysotracker-positive punctate structures of homogeneous size were clearly visible in control cells and were concentrated in the area at the center of the ventral disk (arrow), in PPMP-treated samples, this characteristic pattern was not observed (dashed arrow). Instead, large structures often located at the posterior side of the cell were labeled (arrowhead), most likely corresponding to the large vacuoles observed by transmission electron microscopy analysis.

We then analyzed whether the altered distribution of CLH and lysotracker-positive structures observed upon PPMP treatment were linked to changes in the parasite's ability for endocytosis. To this end, we monitored the internalization of CTX bound to the plasma membrane of trophozoites. In mammalian cells, CTX binds to the raft-associated sphingolipid GM1 and enters the cell by retrograde transport in the endocytic pathway (35). At 4°C, CTX equally labeled the plasma membrane of both control parasites and parasites treated with PPMP for 30 min or 16 h, suggesting that the inhibitor did not alter GM1 presence on the plasma membrane at the concentration and incubation time used here (Fig. 7C). Following incubation at 37°C, CTX was internalized, showing a punctate pattern reminiscent of PVs. In particular, CTX stained the isolated area at the center of the ventral disk in a time-dependent manner (Fig. 7C, arrow). Importantly, enumeration of cells showing this endocytosis signature site revealed that CTX was endocytosed in cells treated with PPMP for 30 min (Fig. 7D, part a) or 16 h (Fig. 7D, part b) with a kinetic similar to control

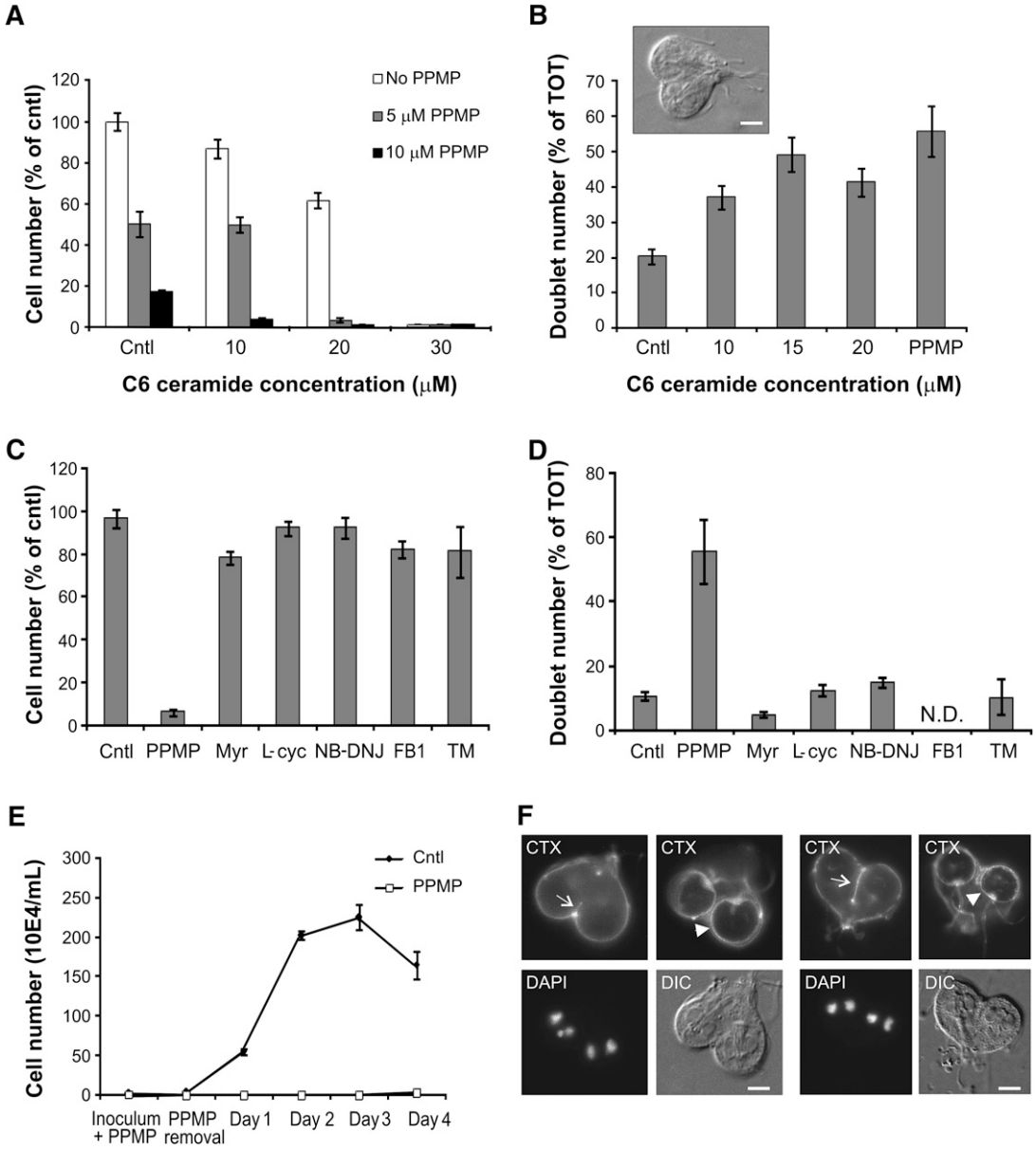

Fig. 5. Ceramide modulates *G. lamblia* cell division. A: Freshly inoculated cultures were treated for 16 h with solvent (cntl) or the indicated concentrations of C6 ceramide in absence (white bars) or presence of 5 μM (gray bars) or 10 μM (black bars) PPMP. Parasites were then harvested and counted; cell numbers are expressed as percentage of untreated samples (cntl). Data are average ± SE (n = 6) of two experiments done in triplicate. Note the agonistic inhibition of parasite replication of C6 ceramide and PPMP. B: Parasite cultures were treated with the indicated concentrations of C6 ceramide and 10 μM PPMP and incompletely divided parasites (doublets) were counted. Results are presented as percentage of total parasite number (TOT) ± SE (n = 6) of two experiments done in triplicate. Inset: differential interference contrast (DIC) image of a cell doublet. C: Freshly inoculated cultures were treated for 16 h with solvent (cntl), 10 μM PPMP, 50 μM fumonisin B1 (FB1), 20 μM myriocin (Myr), 500 μM L-cycloserine (L-cyc), 400 μM NB-DNJ, and 60 μM tunicamycin (TM). Cell numbers are expressed as percentage of untreated samples (cntl). Data are average ± SE (n = 9) of three experiments done in triplicate. D: Parasite cultures were treated as above and incompletely divided parasites (doublets) were counted. Doublet number for FB1-treated cells was not determined. Results are presented as percentage of total parasite number (TOT) ± SE (n = 6) of two experiments done in triplicate. E: Freshly inoculated cultures of trophozoites were treated with 10 μM PPMP or solvent (cntl) for 16 h. After drug removal, parasites were enumerated daily for the following four days. Results of a representative experiment are presented as average ± SE (n = 6). F: Parasite cultures were treated with 10 μM PPMP for 16 h and the plasma membrane stained with FITC-conjugated cholera toxin (CTX). Note the properly formed ventral disks (arrowheads) and the absent or incomplete cleavage furrow (arrows) in incompletely divided parasites. Nuclear staining was performed with DAPI. Scale bar: 3 μm.

cells. In addition, mimicking a PPMP-mediated ceramide increase with exogenous C6 ceramide did not compromise CTX endocytosis (data not shown).

Collectively, our data indicate that PPMP incubation profoundly modified the cellular organization of CLH and lysotracker-positive acidic compartments, suggesting functional alteration of PVs. However, neither drug treatment nor exogenous ceramide inhibited endocytosis of membrane-bound CTX, which is consistent with a principal role of PVs in fluid phase endocytosis (39).

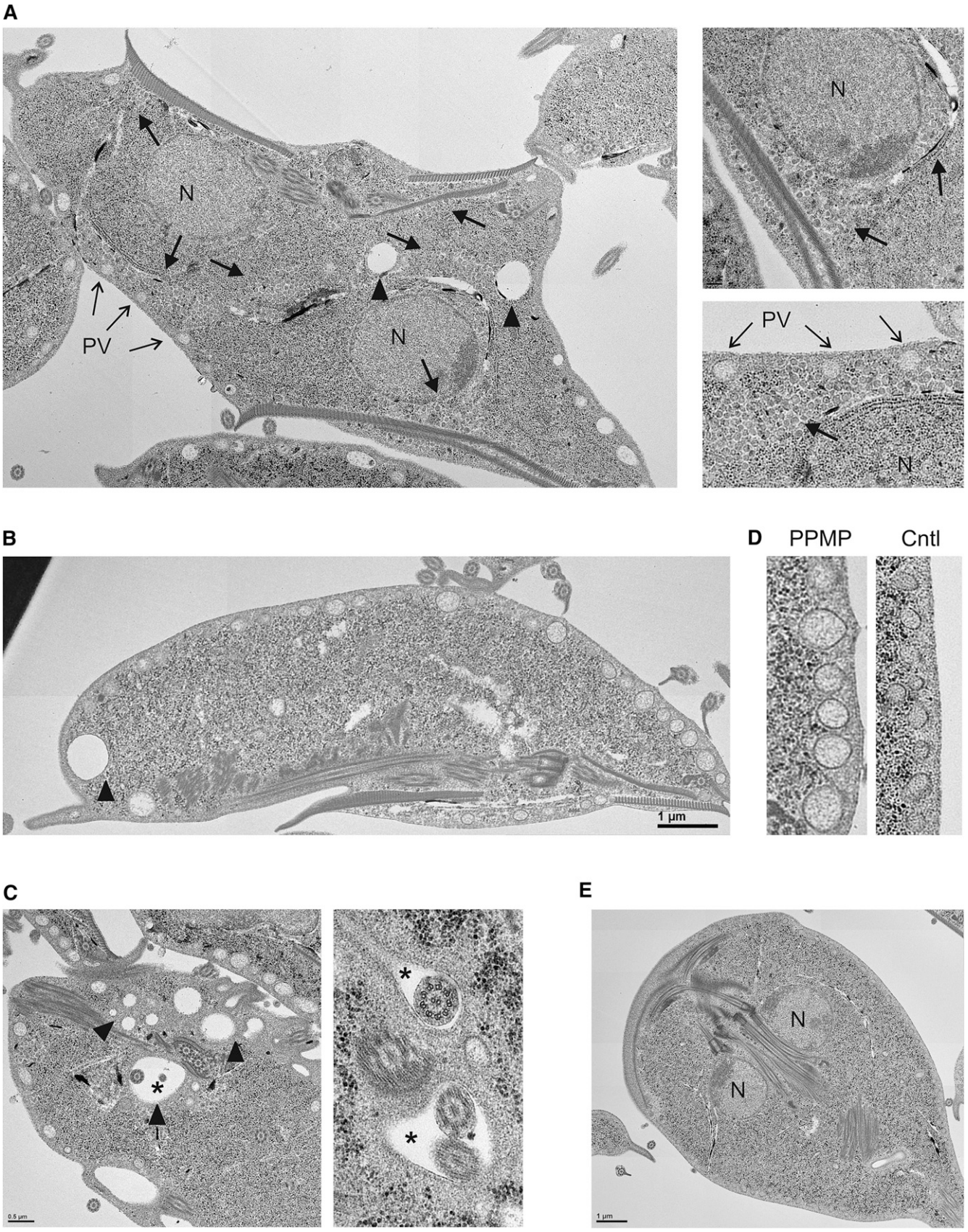

Fig. 6. Ultrastructural abnormalities following inhibition of GlcCer synthesis. Electron micrographs of *G. lamblia* treated with 10 μM PPMP for 16 h. Note the cytosolic accumulation of vesicles (A, thick arrows), the electron-lucent vacuoles of various diameters (A, B, C, arrowheads), the presence of vacuoles containing parasite flagella (C, asterisks), and distended peripheral vesicles (D). Untreated control parasites (E). N, nucleus. PV, peripheral vesicles. Scale bar: 3 μm; except in panel D and right part of panel C, 0.5 μm.

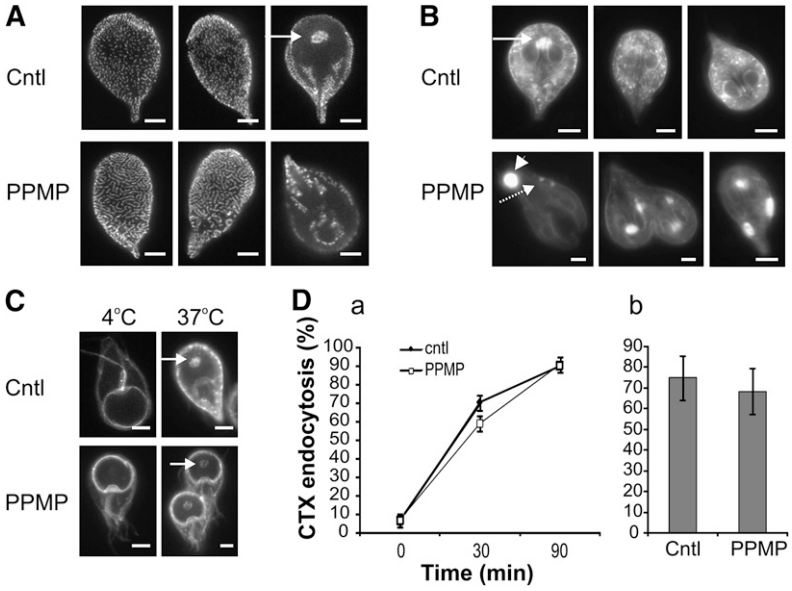

Fig. 7. Inhibition of GlcCer synthesis alters clathrin localization and endolysosomal compartments. A: Parasite cultures were treated with solvent (cntl) or 10 μM PPMP for 16 h and stained with anti-clathrin (CLH) antibody. Note the aggregation of CLH-positive punctuated structures upon PPMP treatment. Arrow, signature site for endocytosis. B: Lysotracker™ staining of acidic compartments in parasites treated as in panel A. Note the reduction of the punctuated staining (dashed arrow) and the appearance of large structures (arrowhead) in PPMP-treated cells. Arrow, signature site for endocytosis. C: Parasite cultures were treated with solvent (cntl) or 10 μM PPMP for 16 h and stained with cholera toxin (CTX) at 4°C to label the plasma membrane. Following a 37°C incubation, CTX is internalized and labels the endocytosis signature site (arrow) in both control and drug treated samples. D. (a) Time course of cells treated for 30 min with 10 μM PPMP, stained with CTX at 4°C and showing the endocytosis signature site following a 37°C incubation for the indicated time. (b) Cells were treated with 10 μM PPMP for 16 h, labeled with CTX as before and counted for endocytosis signature site-staining after 90 min of 37°C incubation. Results are presented as percentage of total parasite number ± SE (n = 6) of two experiments done in triplicate. Scale bars: 3 μm.

Inhibition of GlcCer synthesis reduces both synthesis and trafficking of encystation specific proteins

We previously reported that PPMP treatment affected stage differentiation of *G. lamblia* by inhibiting cyst formation (6). We analyzed the molecular mechanisms of PPMP-mediated inhibition of parasite differentiation in more detail. Lipid metabolic analyses of parasites induced to encyst for 16 h or 24 h revealed that, similar to trophozoites, sphingolipid synthesis was perturbed in presence of PPMP, resulting in decreased GlcCer levels (**Fig. 8A**) and accumulation of ceramide (data not shown).

Next we monitored whether PPMP affects the fate of cyst wall protein 1 (CWP1), a structural protein whose expression, intracellular trafficking, and secretion to form the protective cyst wall are key steps during the encystation process. To quantitatively assess the effect of PPMP on induction of CWP1 synthesis in encysting cells in vitro, we performed population-wide analysis of protein expression by flow cytometry 16 h after induction of differentiation. Control cells showed an expected substantial increase in CWP1 fluorescence compared with trophozoites, indicative of protein expression during encystation (Fig. 8B). Conversely, PPMP-treated cells presented only a modest increase in CWP1 fluorescence, indicating that PPMP severely impaired induction of differentiation.

Next we tested whether PPMP treatment not only inhibited CWP1 expression but also altered the protein's intracellular distribution. Immunofluorescence analysis of encysting parasites showed that in control cells the protein was mainly localized in doughnut-shaped encystation-specific vesicles (ESV) (Fig. 8C). However, in the minor proportion of PPMP-treated cells that showed detectable CWP1 levels, the protein was localized in numerous elongated structures throughout the cell. Dual staining with the ER-resident protein PDI2 revealed that CWP1-positive structures partially colocalized with the ER.

To investigate whether the altered organelle distribution of CWP1 was a specific consequence of PPMP treatment or a general effect resulting from inhibition of parasite replication and CWP1 synthesis, we blocked *G. lamblia* replication with nocodazole (40) and monitored the effect on CWP1 localization. Exposure to 6 μM nocodazole during the first 16 h of the encystation process inhibited not only replication but also CWP1 synthesis at levels comparable with PPMP treatment (supplementary Fig. VI). Microscopic analysis showed that nocodazole-treated parasites were morphologically altered, losing their drop-like shape and becoming round with enlarged nuclei. However, in a minor proportion of cells that showed the CWP1 signal, the protein was localized in vesicular structures with typical ESV morphology (Fig. 8D). As in normal conditions at this stage of differentiation,

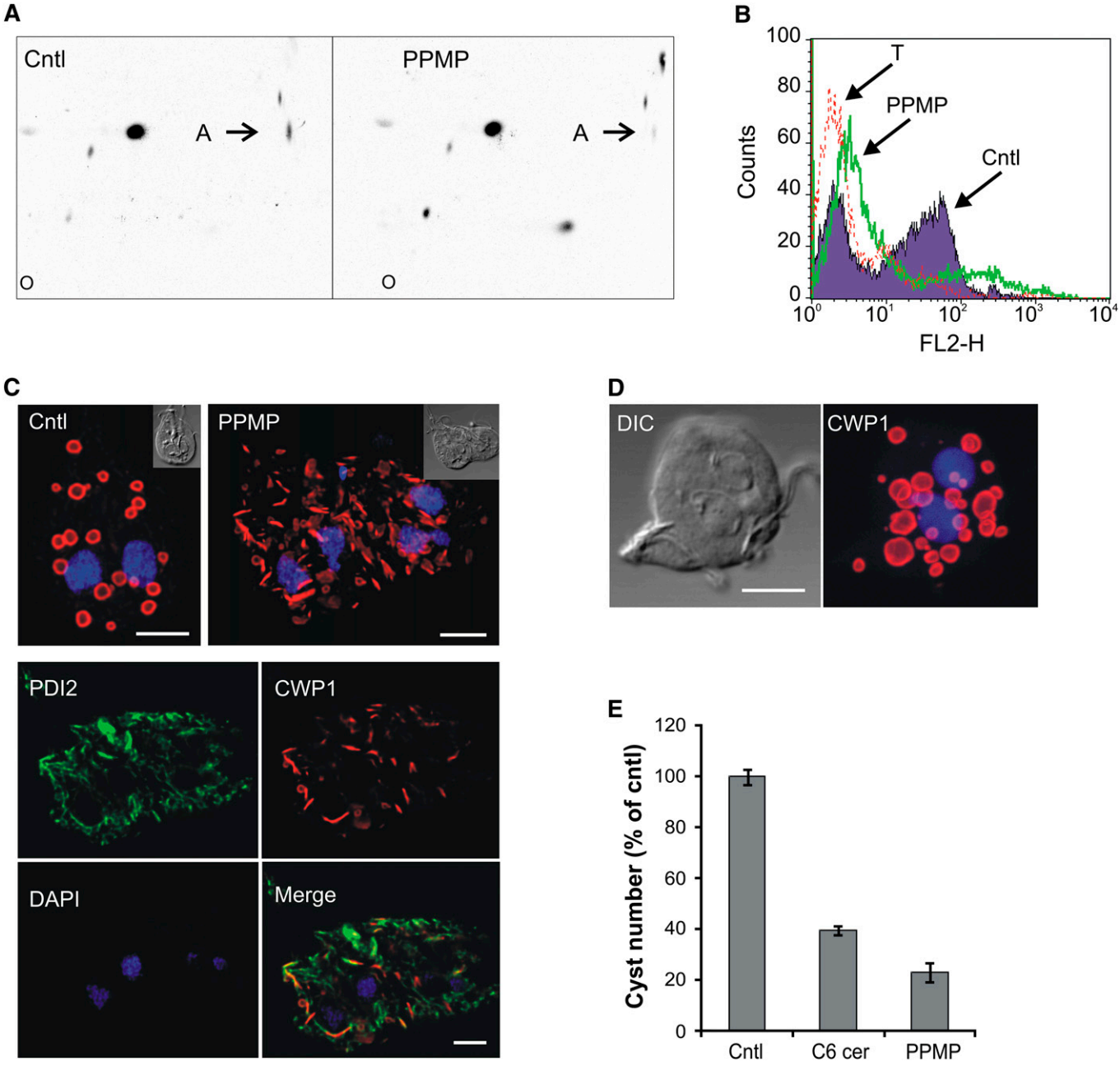

Fig. 8. Inhibition of GlcCer synthesis perturbs CWP1 trafficking. A: Parasites were isolated 24 h after induction of encystation and labeled with [^{3}H]palmitic acid for 3 in presence of 10 μM PPMP or solvent (cntl). Lipid aliquots corresponding to equal protein amount were separated by 2D-HPTLC using the solvent system A. Note the decreased GlcCer levels (spot A) in presence of the inhibitor. B: FACS analysis of parasites encysted for 16 h in presence of solvent (cntl) or 10 μM PPMP and stained for CWP1. Note the modest CWP1 expression in PPMP-treated samples. T, CWP1-stained trophozoites, used as negative control of CWP1 expression. C: Fluorescence analysis of parasites encysted for 16 h in presence of 10 μM PPMP or solvent (cntl) and stained for CWP1 (red), ER-marker PDI1 (green) and nuclei (blue). Upper images, maximum projections; lower images, single optical sections of the deconvolved image stacks. Insets: differential interference contrast (DIC) images. Note the colocalization of CWP1 and PDI2 in PPMP-treated samples. D: Fluorescence analysis of parasites encysted for 16 h in presence of 6 μM nocodazole and stained for CWP1 (red) and nuclei (blue). DIC, differential interference contrast image. Scale bars: 3 μm. E: Parasites were encysted for 16 h in presence of 10 μM PPMP, 20 μM C6 ceramide or solvent (cntl) and stained for CWP1. Cyst number (out of the total cell number) is presented as percentage of control ± SE (n = 3) of a representative from two experiments done in triplicate.

no CWP1 was observed in the ER (data not shown). Collectively, these data suggest that PPMP treatment specifically impaired not only the induction of CWP1 synthesis but also the trafficking of the protein from the ER to the cell surface.

Finally, we tested whether the observed inhibition of *G. lamblia* encystation derived from ceramide accumulation following PPMP treatment. Increasing the cellular levels of this lipid using cell-permeable C6 ceramide potently reduced cyst formation (Fig. 8E), suggesting that inhibition of encystation following PPMP treatment is likely mediated by ceramide buildup in the parasite.

Molecular characterization of *G. lamblia* GCS

Because PPMP's inhibitory effect is known to occur via targeting and inhibition of GlcCer synthase, and a putative GlcCer synthase (GlGCS) homolog is annotated in the *G. lamblia* genome (GL50803_11642), we then focused on characterization of the parasite enzyme. A BLAST database search revealed a number of sequence similarities to deduced amino acid sequences of known GCS and showed a high homology to plant enzymes in terms of amino acid identity, protein length (**Fig. 9A**; supplementary Fig. VII), and hydrophobicity profile (data not shown). Sequence analysis and biochemical data indicated that mammalian GCS belongs to the β-glycosyltransferase family 2 and is a Golgi-resident type III integral membrane protein with a noncleavable N-terminal signal sequence, which serves as a transmembrane anchor, and a long cytoplasmic domain containing the enzyme active site (reviewed in Ref. 41). Sequence alignment with selected GCS members indicated that signature sequences of the family are conserved in *G. lamblia* GCS, including a putative N-terminal transmembrane domain and a long cytosolic domain (Fig. 9A). Importantly, the *G. lamblia* sequence contains the D1, D2, D3, and (Q/R)*XX*RW motifs, which are considered essential for catalytic activity (42). As in the case of mammalian GCS, additional hydrophobic regions are located near the C terminus. While various programs for protein secondary structure prediction (e.g., TMpred) predict transmembrane domains in this region of mammalian GCS, no empirical studies have been performed to determine the exact topology of this GCS region (42).

Mammalian GCS is a Golgi-resident integral membrane protein (41). As *G. lamblia* lacks an identifiable Golgi apparatus (28) but produces developmentally regulated organelles (ESVs) with Golgi-like characteristics (21), we analyzed the localization of GCS in this parasite. To this aim, recombinant GlGCS fused to a C-terminal HA tag was expressed in transgenic parasites. Immunofluorescence analysis of stable integrants revealed an intracellular punctuated signal reminiscent of ER pattern (Fig. 9B). Coimmunostaining of the ER-resident protein PDI2 confirmed that GlGCS colocalized to PDI2-positive ER structures in encysting trophozoites (Fig. 9B, part a). Conversely, coimmunostaining of the encystation-specific protein CWP1 revealed absence of colocalization with GlGCS, indicating that the protein is excluded from ESVs (Fig. 9B, parts b, c).

To investigate the nature of the first N-terminal hydrophobic sequence, HA tags were introduced at the N-terminal end either of the full-length GlGCS or of a variant lacking the first hydrophobic stretch (aa 3–22). Both reporters showed an equivalent signal and distribution, indicating that, like the mammalian homolog, the parasite protein is not proteolytically processed to remove the first hydrophobic sequence (data not shown). Similar results were obtained with HA tagging of the full-length protein at the C-terminus, suggesting that the tag position does not affect the expression or localization of the recombinant protein (data not shown).

G. lamblia GCS regulation during encystation

To investigate whether GlGCS is regulated during parasite stage differentiation, we analyzed the levels of GlGCS mRNA in encysting cells at 7 h after induction, the time when RNA transcription of encystation-specific genes peaks (21). Microarray analysis showed a significant increase of mRNA for the sphingolipid synthesis enzymes GlGCS and serine palmitoyltransferase 2 in encysting cells compared with trophozoites (**Fig. 10A**). The same RNA samples were also processed for semiquantitative real-time PCR (Fig. 10B). The analysis revealed that GlGCS mRNA was less abundant than actin mRNA in both trophozoites and encysting cells (actin:GCS ratio < 1). Consistent with the microarray data, GlGCS mRNA levels increased in encysting cells compared with trophozoites, although the observed 2-fold upregulation was of moderate proportion relative to the considerable 60-fold upregulation of CWP1 mRNA. Thus, higher concentrations of GlGCS mRNA were detected at 7 h encystation using two independent methods, suggesting increased GlGCS activity during parasite stage differentiation. However, contrary to a previous report showing GlcCer accumulation within the cysts by lipid immunostaining (9), our metabolic labeling and lipid analysis did not show increased levels of GlcCer during encystation (Fig. 10C). To determine whether the sphingolipid composition differed during parasite stage-conversion, lipids were extracted from trophozoites and encysting cells and compared by LC-MS. The analysis revealed that GlcCer levels were comparable in the two stages of the parasite; however, the amount of complex glycosphingolipids and in particular of ceramide trihexoside increased considerably in encysting cells (Fig. 10D), revealing that the glycosphingolipid composition of the parasite changed during stage conversion.

Finally, as we showed that both GCS mRNA and complex sphingolipid synthesis are upregulated during stage conversion, we hypothesized that GCS overexpression would promote parasite encystation. To test this, we assessed encystation efficiency in transgenic parasites harboring extra copies of GCS. The analysis revealed that GCS overexpression increased the production of cysts compared with control parasites (Fig. 10E), suggesting that GCS activity is sufficient to promote the encystation process in this parasite.

DISCUSSION

GCS is a pivotal enzyme in the sphingolipid biosynthetic pathway, acting both as a hub for the synthesis of more complex glycosphingolipids and as a regulator of cellular ceramide levels. In the present study, the role of GCS in the cell cycle and stage differentiation of the pathogenic parasite *G. lamblia* was investigated. We found that pharmacological inhibition of GlcCer synthesis increased the cellular levels of ceramide and consequently inhibited cellular proliferation and cytokinesis. In addition, GCS inhibition correlated with intracellular trafficking defects

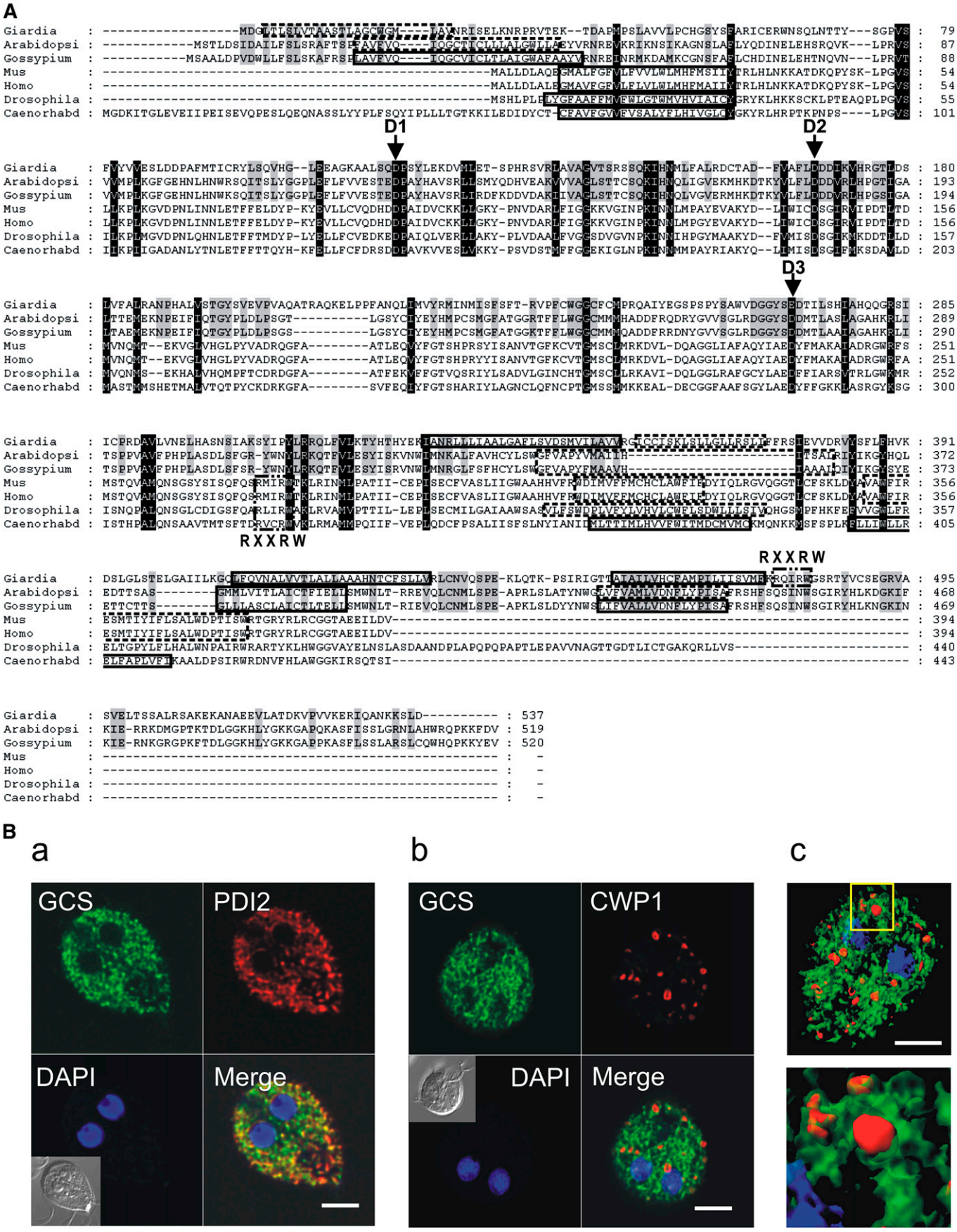

Fig. 9. Giardial GCS belongs to the β-glycosyltransferase family 2 and localizes into ER. A: Protein sequence alignment of GCS orthologs. Black or gray shading indicates highly conserved amino acids among all the sequences or between *G. lamblia* and plant GCS, respectively.

leading to abortive encystation, indicating that GCS plays a crucial role in parasite differentiation.

GlcCer biosynthesis

In mammalian cells, PPMP blocks the synthesis of GlcCer by occupying the catalytic site of GCS. In this study we characterized the GlcCer synthesis in *G. lamblia* and its inhibition by PPMP. We found that an active GCS homolog is present in the parasite and that sphingolipid synthesis can also be targeted by the inhibitor in this organism. As in mammalian cells, inhibition of giardial GCS reduced GlcCer synthesis and induced ceramide accumulation. In addition, GCS inhibition increased the overall lipid turnover in the parasite and, similar to previous observations in mammalian cells (43), increased the synthesis of the neutral lipid DAG. Enhanced neutral lipid synthesis may partially offset the effects on membrane structure caused by a reduced GlcCer formation; alternatively, DAG accumulation may also be the byproduct of increased sphingomyelin synthesis, attempting to lower the levels of ceramide. In support of this hypothesis, exogenously provided ceramide also increased DAG synthesis, suggesting that the altered neutral lipid synthesis is a compensation mechanism for modulating the cellular content of ceramide.

While the synthesis of GlcCer was clearly demonstrated in the parasite by metabolic labeling with radioactive palmitic acid and glucose, the absence of labeled ceramide when supplying the parasites with [^{3}H]serine supported the notion that the sphingolipid synthetic pathway is incomplete in *G. lamblia* and that the parasite uses host-derived ceramide as a substrate for the synthesis of complex sphingolipids. Thus, similar to remodeling of phospholipids in *Giardia* (18), deacylation/reacylation of pre-existing ceramide pools is likely to account for the observed [^{3}H]palmitic acid labeling of ceramide. However, it should be noted that serine incorporation in the parasite was three times less efficient than palmitic acid. This reduced efficiency, combined with the fact that serine is preferentially incorporated into glycerol-based lipids rather than sphingolipids in mammalian cells (44), may be a limiting factor in visualizing sphingolipids in *G. lamblia*. Hence, additional labeled precursors should be used to elucidate the lipid synthetic steps that are active in the parasite. Intriguingly, while a ceramide synthase is not annotated in the *G. lamblia* genome database, the predicted gene product of GL50803_5939 contains a TLC [TRAM/Lag1p/CLN8 (ceroid-lipofuscinoses, neuronal 8)] homology domain (SMART accession number SM00724), which is typical of the Lass (longevity-assurance homolog) family members. Lass proteins, homologs to the yeast Lag1p/Lac1p, are highly conserved among eukaryotes and function in ceramide synthesis (reviewed in Ref. 45). Thus, this *G. lamblia* protein is worthy of careful characterization to elucidate whether ceramide synthase activity is indeed present in the parasite.

Our metabolic analyses showed that of all the sphingolipid inhibitors tested, PPMP was the only compound able to inhibit GlcCer synthesis in *G. lamblia*. This lack of effect of other sphingolipid inhibitors on *G. lamblia* lipid synthesis can be explained by (i) highly divergent parasite enzymes not efficiently recognized by the inhibitory compounds; (ii) poor inhibitor permeability, as described for fumonisin B1 (31); or (iii) incomplete parasite synthetic pathways lacking the enzymes targeted by the used compounds. Of particular interest is the fact that the imino sugar NB-DNJ, a GCS inhibitor structurally unrelated to PPMP, did not affect GlcCer synthesis in *G. lamblia*. NB-DNJ, a promising compound in mammalian cells that is able to reduce GlcCer synthesis, is currently used as a substrate reduction therapy drug for treating type I Gaucher disease (46). However, this inhibitor is not fully specific, as it inhibits β-glycosidase I and II as well as GCS, and it is a much less effective inhibitor of GCS in vitro than the PDMP class of compounds (42). In addition, NB-DNJ has been reported to reduce GlcCer levels not only by inhibiting GCS but also by promoting GlcCer catabolism, acting as a chemical chaperone of GlcCerase (47). Thus the still undefined presence of GlcCerase in the parasite and its efficient targeting by NB-DNJ may be crucial for the GlcCer reduction in *G. lamblia*.

On the other hand, the increased GlcCer synthesis in the parasite following tunicamycin treatment was quite unexpected. In mammalian cells, synthesis of different sphingolipids is compartmentalized, with GlcCer synthesis occurring at the cytosolic face of Golgi membranes and complex sphingolipids at the Golgi lumenal side. In vivo and in vitro experiments showed that tunicamycin inhibits transport of the nucleotide-sugar UDP-Gal into the Golgi, and as a consequence, synthesis of complex sphingolipids in the Golgi lumenal decreased and the precursor GlcCer accumulated (32–34). It is not known whether tunicamycin affects nucleotide-sugar transporter activities in *G. lamblia*. However, a single nucleotide-sugar transporter specific for UDP-GlcNAc was recently described in *G. lamblia*, and interestingly, this sugar was preferentially incorporated into glycolipids rather than into proteins (48). As tunicamycin is a UDP-GlcNAc analog, it is possible that this compound may target the parasite transporter. Thus, the GlcCer accumulation observed in *G. lamblia* following tunicamycin treatment suggests that sphingolipid synthesis may also be compartmentalized in this parasite. This possibility is quite interesting as such a compartmentalization would be likely to occur not in the Golgi

Indicated are the D1,D2,D3,Q/R*XX*RW motifs, which are essential for enzyme activity as demonstrated by site-directed mutagenesis of mammalian GCS. PSORTII predicted transmembrane domains are boxed with solid (strict cutoff) or dashed (loose cutoff) lines. Alignments were performed with Multalin (http://bioinfo.genopole-toulouse.prd.fr/multalin/) and shading was produced with GeneDoc (http://www.psc.edu/biomed/genedoc). B: Fluorescence analysis of parasites expressing recombinant giardial GCS fused to a C-terminal HA tag (green) and encysted for 16 h. Cells were costained for ER-marker PDI2 (part a, red), CWP1 (part b, red), and nuclei (blue). Insets: differential interference contrast (DIC) images. Note the GCS colocalization with the ER marker PDI2 and the absence of colocalization with CWP1. (c) Isosurface model of deconvolved confocal image stack showing giardial GCS (green) and CWP1 (red). Scale bars: 3 μm.

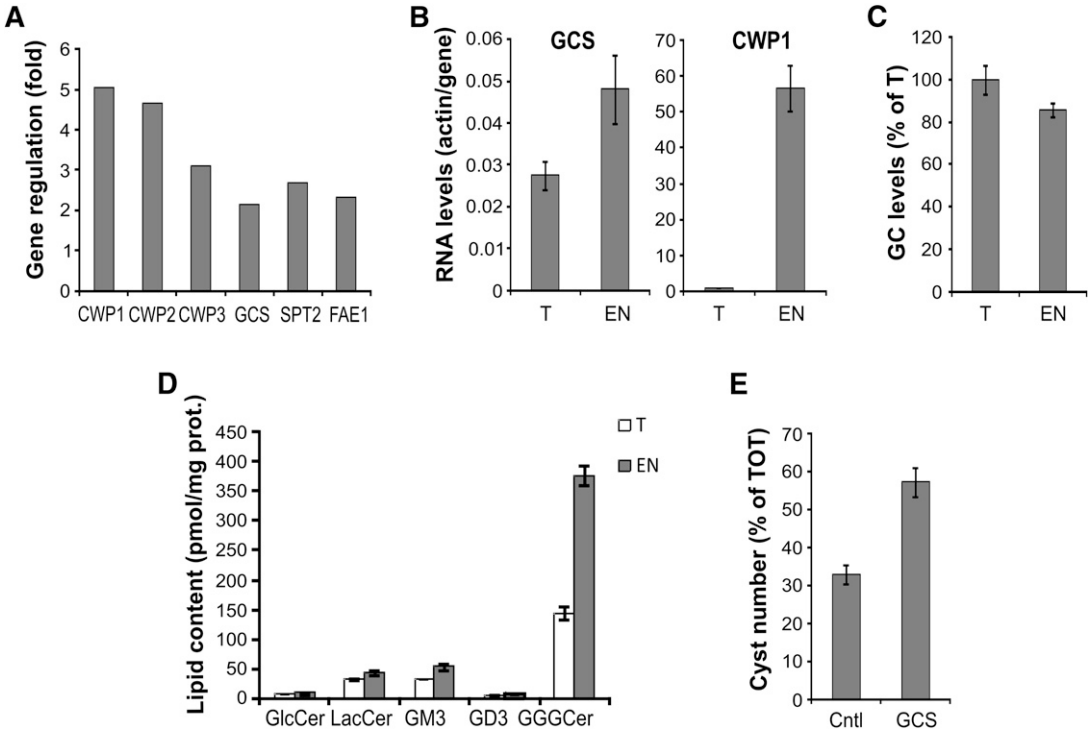

Fig. 10. Giardial GCS is upregulated during parasite stage conversion. A: Microarray analysis at 7 h encystation showing upregulation of the sphingolipid synthesis enzymes GCS and serine palmitoyltransferase 2 compared with trophozoites. Upregulation of cyst wall proteins is shown as positive control. Gene loci are the following: cyst wall protein 1 (CWP1, GL50803_5638), cyst wall protein 2 (CWP2, GL50803_5435), cyst wall protein 3 (CWP3, GL50803_2421), glucosyceramide synthase (GCS, GL50803_11642), serine palmitoyltransferase 2 (SPT2, GL50803_14374), fatty acid elongase 1 (FAE1, GL50803_92729). B: Semiquantitative real-time PCR indicating the upregulation of GCS and CWP1 at 7 h encystation (EN) compared with trophozoite samples (T). Gene expression levels were given as values in arbitrary units relative to the amount of the constitutively expressed house-keeping gene actin. Data are average ± SE (n = 3) of a representative from two experiments done in triplicate. C: Isolated trophozoites (T) or parasites encysted for 24 h (EN) were labeled with 4 μCi/ml of [^{3}H]palmitic acid for 3 h in supplemented PBS. Lipid aliquots corresponding to equal protein amount were separated by 2D-HPTLC using the solvent systems A. Glucosylceramide (GC) levels were expressed as percentage of trophozoite levels; data are average ± SE (n = 3) of a representative from three experiments done in triplicate. D: LC-MS analysis of glycosphingolipids isolated from trophozoites (T) and 24 h encysted cells (EN). GlcCer, glucosylceramide; LacCer, lactosylceramide, GM3 ganglioside (sialic acid, galactosyl-, glucosylceramide), GD3 ganglioside (sialic acid, sialic acid, galactosyl-, glucosylceramide); GGGCer, ceramide trihexoside. Data are average ± SE (n = 3) of a representative from two experiments done in triplicate. E: Parasites expressing recombinant giardial GCS or an empty plasmid (cntl) were encysted for 16 h and stained for CWP1. Cyst number is presented as percentage of total cell number (TOT) ± SE (n = 3) of a representative from three experiments done in triplicate.

apparatus, which is absent in the parasite (28), but in the ER. In support of this idea, epitope-tagged giardial GCS was localized in the ER and in silico analysis showed a putative cytosolic topology of its active site. Thus, it is likely that GlcCer is synthesized on the cytosolic side of the ER and that its translocation to the luminal side may be necessary for further synthesis of complex sphingolipids. In this context, it is worth mentioning that, while mammalian GCS is located in the Golgi apparatus, the *Drosophila* homolog is also present in ER membranes (49).

Ceramide and cell cycle progression

During the inhibition of GlcCer synthesis, *G. lamblia* progressed through rounds of organelle and DNA replication, but it was prevented from completing cytokinesis and forming a cleavage furrow. A possible explanation for the cytokinesis arrest is that inhibition of GlcCer synthesis alters the formation of sphingolipid-rich domains necessary for cytokinesis signaling (50). However, our results showed that increased ceramide levels alone are sufficient to arrest cytokinesis and to block replication in the parasite, indicating that ceramide has antiproliferative effects in the parasite. Moreover, the agonistic effect of ceramide and GCS inhibition suggested that GCS acts as a buffer for regulating the amount of bioactive ceramide. In this regard, it is interesting to note that the ER, the location of giardial GCS, is likely to be the place where prompt regulation of ceramide levels takes place, as ER structures are indeed the site of ceramide accumulation upon incubation with an exogenous fluorescent analog (15).

Interestingly, a crucial role of GCS in the pathogenesis of a microorganism was also described in the pathogenic fungus *Cryptococcus neoformans*, where GlcCer was found to be a key factor for cell division and virulence (51).

The observed ceramide-mediated inhibitory effects in the parasite following treatment with PPMP is consistent with antiproliferative and proapoptotic effects of PPMP in mammalian cells after inducing buildup of ceramide (52, 53). Studies on the existence of a mechanism similar to apoptosis or programmed cell death (PCD) in *G. lamblia*

are scarce. Morphological features of PCD following proapoptotic drugs, including chromatin condensation, apoptotic bodies, and cytoplasmic vacuolation, have been reported; however, our understanding of PCD in *G. lamblia* is limited as the parasite does not harbor bona fide mitochondria, key components in the apoptotic pathways, and typical PCD-mediating proteins, such as caspases, have not been identified in the parasite genome so far (54). Ceramide is an early mediator of cell cycle arrest and apoptosis, acting upstream of caspase-dependent and independent signaling pathways (reviewed in Ref. 55). Interestingly, putative giardial protein homologs of components of the ceramide signaling cascade, including protein phosphatases PP1, PI3K/AKT, and PP2A (56), are annotated in the *Giardia* genome database, and the latter was shown to be involved in the differentiation process of the parasite (57). Thus it is likely that signaling by ceramide, and possibly by other bioactive sphingolipids, is also highly conserved in this simple eukaryote. In support of this hypothesis, we found that psychosine, a sphingolipid which induces cytokinesis arrest (58) and apoptosis (59) in mammalian cells, also inhibited *G. lamblia* cell division at micromolar concentration (unpublished observations). Collectively, our observations suggest that the parasite cell cycle is highly responsive to variations in the cellular levels of bioactive sphingolipids. As the molecular mechanisms of ceramide signaling in eukaryotic cells remains largely undefined because of the high level of complexity, *G. lamblia* with its simple organization and minimized cellular mechanisms (7) can be exploited as a model system to clarify the core components and processes of the signaling machinery.

Vesicular trafficking

Recent studies on a variety of organisms revealed that vesicular trafficking to the cleavage furrow is an essential process for the completion of cytokinesis (reviewed in Ref. 60). Our ultrastructural analyses of PPMP-treated samples revealed abnormal accumulations of vesicles, whose diameters resembled that of coated vesicles involved in intracellular trafficking. In addition, the observed enlarged acidic compartments and aberrant clathrin organization implied that defects in intracellular trafficking may occur upon GlcCer synthesis inhibition. Ceramide has been proposed to modulate vesicular trafficking in mammalian cells; however, the characteristics of this modulation differed in various experimental conditions. Similar to the "lysosome phenotype" observed in *Giardia*, increased ceramide levels have been shown to promote the formation of endocytic vesicles and to induce enlarged lysosomes (61). Enhanced endocytosis after ceramide increase via sphingomyelin degradation was also reported (62). Conversely, ceramide increase using exogenous ceramide, sphingomyelin degradation, or PDMP-mediated GCS inhibition was shown to compromise fluid-phase endocytosis within minutes and, to a lesser extent, receptor-mediated endocytosis (63). These divergent phenotypes raise the possibility that ceramide may differentially regulate endocytic processes in different cell types. In our experimental conditions, we found that PPMP treatment altered lysosome morphology and clathrin organization but did not reduce or enhance internalization of CTX bound to the plasma membrane. Note that the intracellular transport of CTX does not depend on fluid-phase endocytosis; instead, it requires raft association and involves both clathrin-dependent and independent mechanism of endocytosis (reviewed in Ref. 35). Thus, it is possible that CTX endocytosis in *G. lamblia* occurs via a modality not sensitive to ceramide. However, in light of the fact that fluid-phase and receptor-mediated endocytosis is regulated differently in the parasite (39), we cannot exclude that intracellular ceramide levels do not modulate other *G. lamblia* endocytic processes.

Anterograde trafficking of giardial CWP1, a soluble protein which is synthesized during stage differentiation and sorted at the ER level into encystations-specific vesicles (28), was clearly impaired in presence of PPMP, with consequent reduction of CWP1 deposition on the parasite surface and cyst formation. Importantly, treatment with cell-permeable C6 ceramide also reduced cyst formation, suggesting that increased levels of cytosolic ceramide are sufficient to inhibit the encystation process in *G. lamblia*.

Studies in mammalian cells more consistently show that raised ceramide levels inhibit anterograde trafficking (64–67), suggesting that intracellular ceramide concentration may serve as a general modulator of anterograde membrane trafficking events. While it is possible that increased ceramide levels in the parasite following GCS inhibition compromise CWP1 trafficking, it is also conceivable that the reduced concentration of GlcCer plays a role in the observed inhibition, as suggested by the increased cyst formation observed during GCS overexpression. Indeed, glycosphingolipids, most likely GlcCer, are required for the vesicular pathway from the Golgi complex to the melanosome (reviewed in Ref. 68). The proposed mechanism is that GlcCer on the cytosolic side of Golgi membrane is required for the formation of a functional protein coat and subsequent vesicle budding. Thus it is tempting to speculate that in *G. lamblia* GlcCer synthesized by ER-resident GCS may contribute to anterograde protein trafficking by either forming membrane microdomains required for sorting of cargo proteins or binding to cytosolic proteins, which are necessary for recruiting coat proteins and vesicle budding.

CONCLUSION

We have found several novel aspects of sphingolipid metabolism and regulation in *G. lamblia*. Our work revealed that GlcCer synthesis plays a key role in different essential processes associated with the parasite cell cycle and stage differentiation. We also showed that inhibition of GCS blocks parasite cell division, which, together with the likely pharmacological discrimination due to low level of giardial GCS identity with the mammalian counterparts, validates the potential of this enzyme as a target for drug development. Lastly, the presence of an active GCS and the high responsiveness to ceramide in this divergent parasite support the hypothesis that GlcCer synthesis and bioactive sphingolipids have con-

served functions in the regulation of eukaryotic cell processes. In this context, the simple cellular system of *G. lamblia* offers a new perspective from which to explore in detail the mechanisms of sphingolipid function and signaling.

The authors thank Norman Radin for invaluable advice and discussion and Therese Michel and Eva Dalmau for technical assistance.

REFERENCES

1. Bartke, N., and Y. A. Hannun. 2009. Bioactive sphingolipids: metabolism and function. *J. Lipid Res.* **50(Suppl.):** S91–S96.
2. Liu, Y. Y., T. Y. Han, A. E. Giuliano, and M. C. Cabot. 2001. Ceramide glycosylation potentiates cellular multidrug resistance. *FASEB J.* **15:** 719–730.
3. Lucci, A., W. I. Cho, T. Y. Han, A. E. Giuliano, D. L. Morton, and M. C. Cabot. 1998. Glucosylceramide: a marker for multiple-drug resistant cancers. *Anticancer Res.* **18:** 475–480.
4. Liu, Y. Y., T. Y. Han, J. Y. Yu, A. Bitterman, A. Le, A. E. Giuliano, and M. C. Cabot. 2004. Oligonucleotides blocking glucosylceramide synthase expression selectively reverse drug resistance in cancer cells. *J. Lipid Res.* **45:** 933–940.
5. Bleicher, R. J., and M. C. Cabot. 2002. Glucosylceramide synthase and apoptosis. *Biochim. Biophys. Acta.* **1585:** 172–178.
6. Sonda, S., S. Stefanic, and A. B. Hehl. 2008. A sphingolipid inhibitor induces a cytokinesis arrest and blocks stage differentiation in Giardia lamblia. *Antimicrob. Agents Chemother.* **52:** 563–569.
7. Morrison, H. G., A. G. McArthur, F. D. Gillin, S. B. Aley, R. D. Adam, G. J. Olsen, A. A. Best, W. Z. Cande, F. Chen, M. J. Cipriano, et al. 2007. Genomic minimalism in the early diverging intestinal parasite Giardia lamblia. *Science.* **317:** 1921–1926.
8. Savioli, L., H. Smith, and A. Thompson. 2006. Giardia and Cryptosporidium join the 'Neglected Diseases Initiative'. *Trends Parasitol.* **22:** 203–208.
9. Hernandez, Y., M. Shpak, T. T. Duarte, T. L. Mendez, R. A. Maldonado, S. Roychowdhury, M. L. Rodrigues, and S. Das. 2008. Novel role of sphingolipid synthesis genes in regulating giardial encystation. *Infect. Immun.* **76:** 2939–2949.
10. Mattjus, P. 2009. Glycolipid transfer proteins and membrane interaction. *Biochim. Biophys. Acta.* **1788:** 267–272.
11. Jarroll, E. L., P. J. Muller, E. A. Meyer, and S. A. Morse. 1981. Lipid and carbohydrate metabolism of Giardia lamblia. *Mol. Biochem. Parasitol.* **2:** 187–196.
12. Stevens, T. L., G. R. Gibson, R. Adam, J. Maier, M. Allison-Ennis, and S. Das. 1997. Uptake and cellular localization of exogenous lipids by Giardia lamblia, a primitive eukaryote. *Exp. Parasitol.* **86:** 133–143.
13. Blair, R. J., and P. F. Weller. 1987. Uptake and esterification of arachidonic acid by trophozoites of Giardia lamblia. *Mol. Biochem. Parasitol.* **25:** 11–18.
14. Gibson, G. R., D. Ramirez, J. Maier, C. Castillo, and S. Das. 1999. Giardia lamblia: incorporation of free and conjugated fatty acids into glycerol-based phospholipids. *Exp. Parasitol.* **92:** 1–11.
15. Hernandez, Y., C. Castillo, S. Roychowdhury, A. Hehl, S. B. Aley, and S. Das. 2007. Clathrin-dependent pathways and the cytoskeleton network are involved in ceramide endocytosis by a parasitic protozoan, Giardia lamblia. *Int. J. Parasitol.* **37:** 21–32.
16. Pope-Delatorre, H., S. Das, and L. N. Irwin. 2005. Uptake of [3H]-gangliosides by an intestinal protozoan, Giardia lamblia. *Parasitol. Res.* **96:** 102–106.
17. Ellis, J. E., M. A. Wyder, E. L. Jarroll, and E. S. Kaneshiro. 1996. Changes in lipid composition during in vitro encystation and fatty acid desaturase activity of Giardia lamblia. *Mol. Biochem. Parasitol.* **81:** 13–25.
18. Das, S., C. Castillo, and T. Stevens. 2001. Phospholipid remodeling/generation in Giardia: the role of the Lands cycle. *Trends Parasitol.* **17:** 316–319.
19. Hehl, A. B., M. Marti, and P. Kohler. 2000. Stage-specific expression and targeting of cyst wall protein-green fluorescent protein chimeras in Giardia. *Mol. Biol. Cell.* **11:** 1789–1800.
20. Gillin, F. D., S. E. Boucher, S. S. Rossi, and D. S. Reiner. 1989. Giardia lamblia: the roles of bile, lactic acid, and pH in the completion of the life cycle in vitro. *Exp. Parasitol.* **69:** 164–174.
21. Stefanic, S., L. Morf, C. Kulangara, A. Regos, S. Sonda, E. Schraner, C. Spycher, P. Wild, and A. B. Hehl. 2009. Neogenesis and maturation of transient Golgi-like cisternae in a simple eukaryote. *J. Cell Sci.* **122:** 2846–2856.
22. Jimenez-Garcia, L. F., G. Zavala, B. Chavez-Munguia, P. Ramos-Godinez Mdel, G. Lopez-Velazquez, L. Segura-Valdez Mde, C. Montanez, A. B. Hehl, R. Arguello-Garcia, and G. Ortega-Pierres. 2008. Identification of nucleoli in the early branching protist Giardia duodenalis. *Int. J. Parasitol.* **38:** 1297–1304.
23. Rehrauer, H., S. Zoller, and R. Schlapbach. 2007. MAGMA: analysis of two-channel microarrays made easy. *Nucleic Acids Res.* **35:** W86–W90.
24. Smith, G. K. 2005. Limma: linear models for microarray data. *In* Bioinformatics and Computational Biology Solutions Using R and Bioconductor. R. Gentleman, V. Carey, S. Dudoit, R. Irizarry, W. Huber, editors. Springer, New York. 397–420.
25. Bligh, E. G., and W. J. Dyer. 1959. A rapid method of total lipid extraction and purification. *Can. J. Med. Sci.* **37:** 911–917.
26. Munoz-Olaya, J. M., X. Matabosch, C. Bedia, M. Egido-Gabas, J. Casas, A. Llebaria, A. Delgado, and G. Fabrias. 2008. Synthesis and biological activity of a novel inhibitor of dihydroceramide desaturase. *ChemMedChem.* **3:** 946–953.
27. Merrill, A. H., Jr., M. C. Sullards, J. C. Allegood, S. Kelly, and E. Wang. 2005. Sphingolipidomics: high-throughput, structure-specific, and quantitative analysis of sphingolipids by liquid chromatography tandem mass spectrometry. *Methods.* **36:** 207–224.
28. Marti, M., Y. Li, E. M. Schraner, P. Wild, P. Kohler, and A. B. Hehl. 2003. The secretory apparatus of an ancient eukaryote: protein sorting to separate export pathways occurs before formation of transient Golgi-like compartments. *Mol. Biol. Cell.* **14:** 1433–1447.
29. Rani, C. S., A. Abe, Y. Chang, N. Rosenzweig, A. R. Saltiel, N. S. Radin, and J. A. Shayman. 1995. Cell cycle arrest induced by an inhibitor of glucosylceramide synthase. Correlation with cyclin-dependent kinases. *J. Biol. Chem.* **270:** 2859–2867.
30. Das, S., T. Stevens, C. Castillo, A. Villasenor, H. Arredondo, and K. Reddy. 2002. Lipid metabolism in mucous-dwelling amitochondriate protozoa. *Int. J. Parasitol.* **32:** 655–675.
31. Delgado, A., J. Casas, A. Llebaria, J. L. Abad, and G. Fabrias. 2006. Inhibitors of sphingolipid metabolism enzymes. *Biochim. Biophys. Acta.* **1758:** 1957–1977.
32. Guarnaccia, S. P., J. H. Shaper, and R. L. Schnaar. 1983. Tunicamycin inhibits ganglioside biosynthesis in neuronal cells. *Proc. Natl. Acad. Sci. USA.* **80:** 1551–1555.
33. Yusuf, H. K., G. Pohlentz, and K. Sandhoff. 1983. Tunicamycin inhibits ganglioside biosynthesis in rat liver Golgi apparatus by blocking sugar nucleotide transport across the membrane vesicles. *Proc. Natl. Acad. Sci. USA.* **80:** 7075–7079.
34. Burger, K. N., P. van der Bijl, and G. van Meer. 1996. Topology of sphingolipid galactosyltransferases in ER and Golgi: transbilayer movement of monohexosyl sphingolipids is required for higher glycosphingolipid biosynthesis. *J. Cell Biol.* **133:** 15–28.
35. Lencer, W. I., and D. Saslowsky. 2005. Raft trafficking of AB5 subunit bacterial toxins. *Biochim. Biophys. Acta.* **1746:** 314–321.
36. Correa, G., and M. Benchimol. 2006. Giardia lamblia behavior under cytochalasins treatment. *Parasitol. Res.* **98:** 250–256.
37. Granger, B. L., S. J. Warwood, M. Benchimol, and W. De Souza. 2000. Transient invagination of flagella by Tritrichomonas foetus. *Parasitol. Res.* **86:** 699–709.
38. Lanfredi-Rangel, A., M. Attias, T. M. de Carvalho, W. M. Kattenbach, and W. De Souza. 1998. The peripheral vesicles of trophozoites of the primitive protozoan Giardia lamblia may correspond to early and late endosomes and to lysosomes. *J. Struct. Biol.* **123:** 225–235.
39. Gaechter, V., E. Schraner, P. Wild, and A. B. Hehl. 2008. The single dynamin family protein in the primitive protozoan Giardia lamblia is essential for stage conversion and endocytic transport. *Traffic.* **9:** 57–71.
40. Mariante, R. M., R. G. Vancini, A. L. Melo, and M. Benchimol. 2005. Giardia lamblia: evaluation of the in vitro effects of nocodazole and colchicine on trophozoites. *Exp. Parasitol.* **110:** 62–72.
41. Ichikawa, S., and Y. Hirabayashi. 1998. Glucosylceramide synthase and glycosphingolipid synthesis. *Trends Cell Biol.* **8:** 198–202.
42. Marks, D. L., M. Dominguez, K. Wu, and R. E. Pagano. 2001. Identification of active site residues in glucosylceramide synthase.

A nucleotide-binding catalytic motif conserved with processive beta-glycosyltransferases. *J. Biol. Chem.* **276:** 26492–26498.
43. Radin, N. S. 1994. Rationales for cancer chemotherapy with PDMP, a specific inhibitor of glucosylceramide synthase. *Mol. Chem. Neuropathol.* **21:** 111–127.
44. Andrade, C. M., V. M. Trindade, C. C. Cardoso, A. L. Ziulkoski, L. C. Trugo, R. M. Guaragna, R. Borojevic, and F. C. Guma. 2003. Changes of sphingolipid species in the phenotype conversion from myofibroblasts to lipocytes in hepatic stellate cells. *J. Cell. Biochem.* **88:** 533–544.
45. Teufel, A., T. Maass, P. R. Galle, and N. Malik. 2009. The longevity assurance homologue of yeast lag1 (Lass) gene family. [Review] *Int. J. Mol. Med.* **23:** 135–140.
46. Cox, T. M. 2005. Substrate reduction therapy for lysosomal storage diseases. *Acta Paediatr. Suppl.* **94:** 69–75; discussion 57.
47. Alfonso, P., S. Pampin, J. Estrada, J. C. Rodriguez-Rey, P. Giraldo, J. Sancho, and M. Pocovi. 2005. Miglustat (NB-DNJ) works as a chaperone for mutated acid beta-glucosidase in cells transfected with several Gaucher disease mutations. *Blood Cells Mol. Dis.* **35:** 268–276.
48. Banerjee, S., J. Cui, P. W. Robbins, and J. Samuelson. 2008. Use of Giardia, which appears to have a single nucleotide-sugar transporter for UDP-GlcNAc, to identify the UDP-Glc transporter of Entamoeba. *Mol. Biochem. Parasitol.* **159:** 44–53.
49. Kohyama-Koganeya, A., T. Sasamura, E. Oshima, E. Suzuki, S. Nishihara, R. Ueda, and Y. Hirabayashi. 2004. Drosophila glucosylceramide synthase: a negative regulator of cell death mediated by proapoptotic factors. *J. Biol. Chem.* **279:** 35995–36002.
50. Ng, M. M., F. Chang, and D. R. Burgess. 2005. Movement of membrane domains and requirement of membrane signaling molecules for cytokinesis. *Dev. Cell.* **9:** 781–790.
51. Rittershaus, P. C., T. B. Kechichian, J. C. Allegood, A. H. Merrill, Jr., M. Hennig, C. Luberto, and M. Del Poeta. 2006. Glucosylceramide synthase is an essential regulator of pathogenicity of Cryptococcus neoformans. *J. Clin. Invest.* **116:** 1651–1659.
52. Chan, S. Y., A. L. Hilchie, M. G. Brown, R. Anderson, and D. W. Hoskin. 2007. Apoptosis induced by intracellular ceramide accumulation in MDA-MB-435 breast carcinoma cells is dependent on the generation of reactive oxygen species. *Exp. Mol. Pathol.* **82:** 1–11.
53. Litvak, D. A., A. J. Bilchik, and M. C. Cabot. 2003. Modulators of ceramide metabolism sensitize colorectal cancer cells to chemotherapy: a novel treatment strategy. *J. Gastrointest. Surg.* **7:** 140–148; discussion 148.
54. Chose, O., C. O. Sarde, C. Noel, D. Gerbod, J. C. Jimenez, C. Brenner, M. Capron, E. Viscogliosi, and A. Roseto. 2003. Cell death in protists without mitochondria. *Ann. N. Y. Acad. Sci.* **1010:** 121–125.
55. Lahiri, S., and A. H. Futerman. 2007. The metabolism and function of sphingolipids and glycosphingolipids. *Cell. Mol. Life Sci.* **64:** 2270–2284.
56. Ogretmen, B., and Y. A. Hannun. 2004. Biologically active sphingolipids in cancer pathogenesis and treatment. *Nat. Rev. Cancer.* **4:** 604–616.
57. Lauwaet, T., B. J. Davids, A. Torres-Escobar, S. R. Birkeland, M. J. Cipriano, S. P. Preheim, D. Palm, S. G. Svard, A. G. McArthur, and F. D. Gillin. 2007. Protein phosphatase 2A plays a crucial role in Giardia lamblia differentiation. *Mol. Biochem. Parasitol.* **152:** 80–89.
58. Kozutsumi, Y., T. Kanazawa, Y. Sun, T. Yamaji, H. Yamamoto, and H. Takematsu. 2002. Sphingolipids involved in the induction of multinuclear cell formation. *Biochim. Biophys. Acta.* **1582:** 138–143.
59. Giri, S., M. Khan, R. Rattan, I. Singh, and A. K. Singh. 2006. Krabbe disease: psychosine-mediated activation of phospholipase A2 in oligodendrocyte cell death. *J. Lipid Res.* **47:** 1478–1492.
60. Albertson, R., B. Riggs, and W. Sullivan. 2005. Membrane traffic: a driving force in cytokinesis. *Trends Cell Biol.* **15:** 92–101.
61. Li, R., E. J. Blanchette-Mackie, and S. Ladisch. 1999. Induction of endocytic vesicles by exogenous C(6)-ceramide. *J. Biol. Chem.* **274:** 21121–21127.
62. Zha, X., L. M. Pierini, P. L. Leopold, P. J. Skiba, I. Tabas, and F. R. Maxfield. 1998. Sphingomyelinase treatment induces ATP-independent endocytosis. *J. Cell Biol.* **140:** 39–47.
63. Chen, C. S., A. G. Rosenwald, and R. E. Pagano. 1995. Ceramide as a modulator of endocytosis. *J. Biol. Chem.* **270:** 13291–13297.
64. Rosenwald, A. G., and R. E. Pagano. 1993. Inhibition of glycoprotein traffic through the secretory pathway by ceramide. *J. Biol. Chem.* **268:** 4577–4579.
65. Maceyka, M., and C. E. Machamer. 1997. Ceramide accumulation uncovers a cycling pathway for the cis-Golgi network marker, infectious bronchitis virus M protein. *J. Cell Biol.* **139:** 1411–1418.
66. Giussani, P., M. Maceyka, H. Le Stunff, A. Mikami, S. Lepine, E. Wang, S. Kelly, A. H. Merrill, Jr., S. Milstien, and S. Spiegel. 2006. Sphingosine-1-phosphate phosphohydrolase regulates endoplasmic reticulum-to-golgi trafficking of ceramide. *Mol. Cell. Biol.* **26:** 5055–5069.
67. Nakamura, M., N. Kuroiwa, Y. Kono, and A. Takatsuki. 2001. Glucosylceramide synthesis inhibitors block pharmacologically induced dispersal of the Golgi and anterograde membrane flow from the endoplasmic reticulum: implication of sphingolipid metabolism in maintenance of the Golgi architecture and anterograde membrane flow. *Biosci. Biotechnol. Biochem.* **65:** 1369–1378.
68. van Meer, G., J. Wolthoorn, and S. Degroote. 2003. The fate and function of glycosphingolipid glucosylceramide. *Philos. Trans. R. Soc. Lond. B Biol. Sci.* **358:** 869–873.